Spring 2017

Strategies for high efficiency silicon solar cells

Lauren Michel Davidson
University of Iowa

STRATEGIES FOR HIGH EFFICIENCY SILICON SOLAR CELLS

by

Lauren Michel Davidson

A thesis submitted in partial fulfillment
of the requirements for the Master of Science
degree in Electrical and Computer Engineering in the
Graduate College of
The University of Iowa

May 2017

Thesis Supervisor: Assistant Professor Fatima Toor

Graduate College
The University of Iowa
Iowa City, Iowa

CERTIFICATE OF APPROVAL

_____

MASTER'S THESIS

_____

This is to certify that the Master's thesis of

Lauren Michel Davidson

has been approved by the Examining Committee for
the thesis requirement for the Master of Science degree
in Electrical and Computer Engineering at the May 2017 graduation.

Thesis Committee: _____
Fatima Toor, Thesis Supervisor

_____
Anton Kruger

_____
David Andersen

ACKNOWLEDGMENTS

I would like to thank my advisor Professor Fatima Toor for her productive feedback of my work and her support and encouragement of my project. I am grateful to have had the opportunity to work in her research group. I would also like to thank my coworker Wenqi Duan for all of her help and support in the fabrication process of my project.

ABSTRACT

The fabrication of low cost, high efficiency solar cells is imperative in competing with existing energy technologies. Many research groups have explored using III-V materials and thin-film technologies to create high efficiency cells; however, the materials and manufacturing processes are very costly as compared to monocrystalline silicon (Si) solar cells. Since commercial Si solar cells typically have efficiencies in the range of 17-19%, techniques such as surface texturing, depositing a surface-passivating film, and creating multi-junction Si cells are used to improve the efficiency without significantly increasing the manufacturing costs. This research focused on two of these techniques: (1) a tandem junction solar cell comprised of a thin-film perovskite top cell and a wafer-based Si bottom cell, and (2) Si solar cells with single- and double-layer silicon nitride (SiN_x) anti-reflection coatings (ARC).

The perovskite/Si tandem junction cell was modeled using a Matlab analytical program. The model took in material properties such as doping concentrations, diffusion coefficients, and band gap energy and calculated the photocurrents, voltages, and efficiencies of the cells individually and in the tandem configuration. A planar Si bottom cell, a cell with a SiN_x coating, or a nanostructured black silicon (bSi) cell can be modeled in either an n-terminal or series-connected configuration with the perovskite top cell. By optimizing the bottom and top cell parameters, a tandem cell with an efficiency of 31.78% was reached.

Next, planar Si solar cells were fabricated, and the effects of single- and double-layer SiN_x films deposited on the cells were explored. Silicon nitride was sputtered onto planar Si samples, and the refractive index and thicknesses of the films were measured

using ellipsometry. A range of refractive indices can be reached by adjusting the gas flow rate ratios of nitrogen (N_2) and argon (Ar) in the system. The refractive index and thickness of the film affect where the minimum of the reflection curve is located. For Si, the optimum refractive index of a single-layer passivation film is 1.85 with a thickness of 80nm so that the minimum reflection is at 600nm, which is where the photon flux is maximized. However, using a double-layer film of SiN_x, the Si solar cell performance is further improved due to surface passivation and lowered surface reflectivity. A bottom layer film with a higher refractive index passivates the Si cell and reduces surface reflectivity, while the top layer film with a smaller refractive index further reduces the surface reflectivity. The refractive indices and thicknesses of the double-layer films were varied, and current-voltage (IV) and external quantum efficiency (EQE) measurements were taken. The double-layer films resulted in an absolute value increase in efficiency of up to 1.8%.

PUBLIC ABSTRACT

Commercial monocrystalline silicon solar cells have efficiencies in the range of 17-19%, prompting the research of different manufacturing techniques and processes to increase the efficiency of these cells without significantly increasing the cost. Multi-junction solar cells and the use of textured surfaces and anti-reflection coatings are two of the techniques used to create high efficiency silicon solar cells.

A tandem junction solar cell comprised of a perovskite top cell and silicon bottom cell was modeled using Matlab. By adjusting the material properties and using a nanostructured black silicon bottom cell, the tandem cell reached a theoretical efficiency of greater than 30%. The analytical model results support the shift in solar research towards tandem cells and the use of organic-inorganic materials.

Next, planar silicon solar cells were fabricated, and the effects of silicon nitride anti-reflection coatings were studied. The silicon nitride films act as both an anti-reflection coating and a surface-passivating coating, improving the performance of the cell significantly. By adjusting the refractive indices and thicknesses of the layers, the silicon nitride films can be optimized so that the lowest reflectivity is in the range of wavelengths where the number of incident photons on the cell is maximized. The refractive indices were varied by changing the gas flow rate ratio of nitrogen and argon in the deposition system, resulting in cells that had efficiency increases of up to 1.8%. The optimization of the two techniques presented in this thesis is imperative in the progress towards cost competitive, high efficiency solar cells.

TABLE OF CONTENTS

LIST OF TABLES

LIST OF FIGURES

1. PHYSICS OF SOLAR CELLS

1.1 Introduction

Wafer-based monocrystalline silicon (c-Si) solar cells have plateaued at an efficiency of 25% [1] showing little improvement in recent years. This has prompted the research of different manufacturing techniques and materials to create high efficiency, cost competitive solar cells. Many research groups have explored using III-V materials [2] such as gallium arsenide (GaAs) and indium gallium phosphide (InGaP) to create high efficiency cells. While high efficiency is attainable, up to 40% with GaAs [1], these materials are expensive to manufacture and cannot commercially compete with the cost of Si at $18/kg [3]. Other groups have researched surface passivation through nanostructures and patterned surfaces, such as black silicon (bSi) [4-7]. These nanostructures, which can take the formation of rods, pyramids, inverted pyramids, and even a porous structure, reduce the reflectivity of the surface, allowing more sunlight to be absorbed by the cell. Black silicon (bSi), so called for its black surface, decreases the average reflectivity of Si from 35% to as low as 1.4% [4]; however, its blue light response is poor, which plays a role in its 24% maximum cell efficiency. In order to improve the surface passivation of the cell, rather than just the reflectivity, groups have manufactured cells with an anti-reflective coating (ARC) which also acts as a surface passivation layer. Common thin layers are silicon dioxide (SiO_2) and silicon nitride (SiN_x), but other materials such as titanium oxide (TiO_2) have been used in conjunction with SiO_2 and SiN_x to decrease the reflectivity and increase the surface passivation. Cells with a surface passivation layer such as the ones mentioned above have shown efficiencies of 17-19% [8]. Each of these techniques are discussed in further detail later in this thesis; however, it is important to first understand the physics of a solar cell and how different surfaces and coatings affect the performance of the cell.

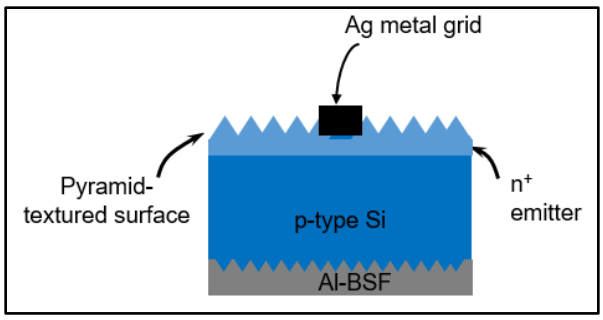

Figure 1. Structure of single junction Si solar cell with surface texturing and Al back surface field.

A typical solar cell follows the structure given in *Figure 1*. The cell consists of a base, emitter, and back surface field (BSF). In the solar cell shown in the above figure, the base, the thickest absorber is a p-type Si substrate, and the emitter is a highly doped n-type Si substrate. The pyramid-textured surface is used to reduce reflection and increase light absorption of the cell. The region where the p-type substrate and the n+ emitter meet is the pn-junction, also known as the space charge region or the depletion region. Photocurrents are developed in all three regions, and the equations used to determine the currents are derived in the next section. The final layer of the cell, is the BSF, which consists of a highly doped material, and in *Figure 1*, is aluminum (Al). The Al BSF is used to reduce rear surface recombination, as well as creating the back contact for the cell. The circuit is completed with a silver (Ag) metal grid, which acts as the top contact of the cell. When a photon is absorbed by the cell, an electron-hole pair is created. The generation rate of the electron-hole pair is quantified by equation (1.1.1), where $\alpha(\lambda)$ is the absorption coefficient, $\phi(\lambda)$ is the number of incident photons per area per time per unit bandwidth, or the photon flux, and $R(\lambda)$ is the reflectivity of the surface at a given wavelength.

$$G(\lambda, x) = \alpha(\lambda)\phi(\lambda)[1 - R(\lambda)]e^{-\alpha(\lambda)x} \qquad (1.1.1)$$

The carriers are collected in the emitter and base regions through a diffusion process [9]. The collection of these carriers generates a current that flows through the cell. Due to the collection of carriers, there is an increase in the number of electrons in the n-type region and an increase in the number of holes in the p-type region. The separation of charge creates an electric field giving way to a voltage potential across the cell. We can model this process with an electric circuit, assuming that the solar cell has ideal diode current-voltage (IV) characteristics [9]. *Figure 2* below shows the

photocurrent modeled as a constant current source in parallel with a diode and series and shunt resistances.

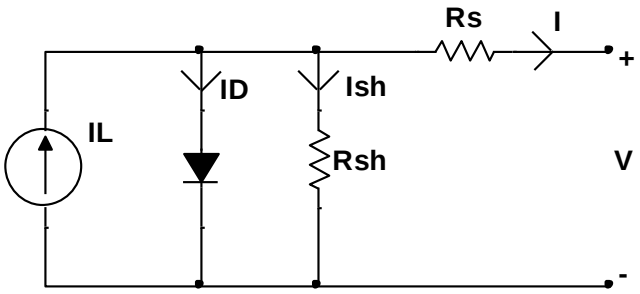

Figure 2. Equivalent circuit of ideal solar cell.

Thus, using circuit analysis, the total current of the cell is given in equation (1.1.2), where the saturation current of the diode is given by equation (1.1.3), and I_L represents the photocurrent.

$$I = I_s\left[e^{\frac{qV}{kT}} - 1\right] - I_L \tag{1.1.2}$$

$$I_s = AqN_CN_V\left(\frac{1}{N_A}\sqrt{\frac{D_n}{\tau_n}} + \frac{1}{N_D}\sqrt{\frac{D_p}{\tau_p}}\right)e^{\frac{-E_g}{kT}} \tag{1.1.3}$$

By setting the current, I, equal to zero, we can find the open circuit voltage, V_{oc}, given by equation (1.1.4).

$$V_{oc} = \frac{kT}{q}\ln\left(\frac{I_L}{I_s} + 1\right) \tag{1.1.4}$$

The short circuit current, I_{sc}, which is the current when the voltage is zero, is given by equation (1.1.5), where IQE(λ) is the internal quantum efficiency of the cell with respect to wavelength.

$$I_{sc} = q\int[1 - R(\lambda)]\phi(\lambda)IQE(\lambda)d\lambda \tag{1.1.5}$$

These equations give the IV characteristics of the solar cell, commonly graphed as shown in *Figure 3*. The multiplication of the maximum current and voltage values gives the maximum power output of the cell. The fill factor is then found by taking the maximum power and dividing it by the multiplication of V_{oc} and I_{sc}, equation (1.1.6).

$$FF = \frac{I_m V_m}{I_{sc} V_{oc}} \tag{1.1.6}$$

The efficiency of the cell is then calculated by dividing the maximum output power by the input power, shown in equation (1.1.7).

$$\eta = \frac{P_m}{P_{in}} \tag{1.1.7}$$

These parameters are commonly used to determine the performance quality of the cell along with the quantum efficiency measurements, discussed in the following section.

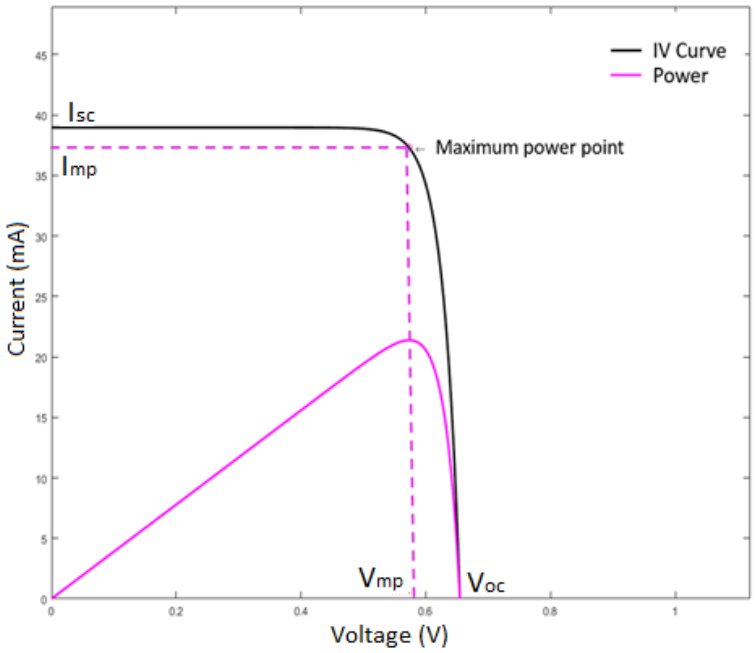

Figure 3. Standard IV and power curves for solar cell. The figure shows the maximum current, voltage, and power points as well as the open circuit voltage and short circuit current values.

1.2 Photocurrent and Spectral Response

The photocurrent that is generated by the collection of carriers is derived for each of the three regions: emitter, base, and space charge region. Assuming abrupt doping profiles $N_D >> N_A$ [9] and low-injection conditions, the one-dimensional, steady-state continuity equations for the electrons and holes are given in the equations (1.2.1) and (1.2.2), respectively.

$$G_n - \left(\frac{n_p - n_{po}}{\tau_n}\right) + \frac{1}{q}\frac{dJ_n}{dx} = 0 \tag{1.2.1}$$

$$G_p - \left(\frac{p_n - p_{no}}{\tau_p}\right) - \frac{1}{q}\frac{dJ_p}{dx} = 0 \tag{1.2.2}$$

The current-density, which is the photocurrent per unit area, is given by equations (1.2.3) and (1.2.4).

$$J_n = q\mu_n n_p \mathcal{E} + qD_n\left(\frac{dn_p}{dx}\right) \tag{1.2.3}$$

$$J_p = q\mu_p p_n \mathcal{E} - qD_p\left(\frac{dp_n}{dx}\right) \tag{1.2.4}$$

Combining the generation rate equation with the continuity equations and current-density equations and applying the appropriate boundary conditions, the photocurrent density equations in the emitter, base, and space charge regions are derived below.

$$J_p = \left[\frac{q\phi(1-R)\alpha L_p}{(\alpha^2 L_p^2 - 1)}\right]\left[\frac{\left(\frac{S_p L_p}{D_p} + \alpha L_p\right) - e^{-\alpha x_j}\left(\frac{S_p L_p}{D_p}\cosh\left(\frac{x_j}{L_p}\right) + \sinh\left(\frac{x_j}{L_p}\right)\right)}{\left(\frac{S_p L_p}{D_p}\right)\sin\left(\frac{x_j}{L_p}\right) + \cosh\left(\frac{x_j}{L_p}\right)} - \alpha L_p e^{-\alpha x_j}\right] \tag{1.2.5}$$

$$J_n = \left[\frac{q\phi(1-R)\alpha L_n e^{-\alpha(x_j+W_D)}}{\alpha^2 L_n^2 - 1}\right]\left[\alpha L_n - \frac{\left(\frac{S_n L_n}{D_n}\right)\left[\cosh\left(\frac{H'}{L_n}\right) - e^{-\alpha H'}\right] + \sinh\left(\frac{H'}{L_n}\right) + \alpha L_n e^{-\alpha H'}}{\left(\frac{S_n L_n}{D_n}\right)\sinh\left(\frac{H'}{L_n}\right) + \cosh\left(\frac{H'}{L_n}\right)}\right] \quad (1.2.6)$$

$$J_{scr} = q\phi(1-R)e^{-\alpha x_j}[1 - e^{-\alpha W_D}] \quad (1.2.7)$$

In the above equations, the absorption coefficient, photon flux, and reflectivity of the surface of the material are dependent upon the wavelength (λ) of light. The spectral response of the cell is therefore dependent upon wavelength as well. Quantum efficiency, or spectral response, is the ratio of the number of collected carriers to the number of photons incident upon the cell [9]. The external quantum efficiency and internal quantum efficiency equations are shown below. The quantum efficiency curves are used to parametrize the optical performance of the cell, indicating recombination effects in both the front surface and rear surface as well as band-edge effects.

$$EQE(\lambda) = \int \frac{J_{ph}(\lambda)}{q\phi(\lambda)} d\lambda \quad (1.2.8)$$

$$IQE(\lambda) = \int \frac{J_{ph}(\lambda)}{q\phi(\lambda)[1 - R(\lambda)]} d\lambda \quad (1.2.9)$$

1.3 Single Junction Cell Model

A single silicon solar was modeled in Matlab using the equations that were given in the previous section. The analytical model allows a user to enter in the different parameters of a material, then calculates the voltage, current, power, and quantum efficiency for that cell. In this section, the simulation results for a single Si cell are discussed; however, in Chapter 2, a tandem junction solar cell comprised of Si and perovskite is modeled, using the same equations as a single cell. *Table 1* and *Table 2* below show the different parameters and constants that are considered when calculating the theoretical performance of the cell.

Table 1. Constants of Matlab model.

Symbol	Parameter	Value
q	Charge of electron	1.602×10^{-19} C
h	Planck constant	6.626×10^{-34} J-s
k	Boltzmann constant	1.3807×10^{-23} J/K
c	Speed of light	299,792,458 m/s
n	Refractive index of air	1

Table 2. Input parameters of Matlab model.

Symbol	Parameter	Units
N_d	Donor density	cm^{-3}
D_p	Hole diffusion coefficient in emitter	cm^2/s
τ_p	Hole life time in emitter	s
L_p	Hole diffusion length in emitter	cm
N_a	Acceptor density	cm^{-3}
D_n	Electron diffusion coefficient in base	cm^2/s
τ_n	Electron life time in base	s
L_n	Electron diffusion length in base	cm
W	Depletion width	cm
H'	Thickness of substrate	cm
x_j	Junction depth of n+ region	cm
S_n	Surface recombination velocity for electrons	cm/s
S_p	Surface recombination velocity for holes	cm/s
E_g	Band gap energy	eV
N_c	Conduction band carrier density	cm^{-3}
N_v	Valence band carrier density	cm^{-3}
T	Temperature	K
H	Total cell thickness	cm

The first single junction solar cell modeled in Matlab was a black silicon (bSi) cell created and tested by Toor et al [4]. The parameters of the cell were entered in the

program in order to test the accuracy of the theoretical model to experimental results. Reflection and absorption data files for bSi were uploaded to the model and then run. The quantum efficiency (QE) curves and IV curves generated by the model were compared with the experimental QE and IV curves. The efficiency, short circuit current, open circuit voltage, and fill factor values were also compared with the experimental data. The model calculated the IV characteristics of the bSi cell as follows: $\eta = 17.27\%$, $V_{oc} = .5956$ V, $J_{sc} = 35.09$ mA/cm^2, and FF = 82.65%. The model efficiency was within 5% of the experimental efficiency value given by Toor et al [4]. The EQE, IQE, and IV curves are shown in the *Figure 4* below. Once the model accuracy was confirmed, single junction solar cells using planar Si with a SiN_x AR coating were analyzed. The accuracy of the single junction cell model built confidence in the tandem junction solar cell model, since it is based on the same principles as the single junction model. The tandem junction model is discussed further in Chapter 2.

(a)

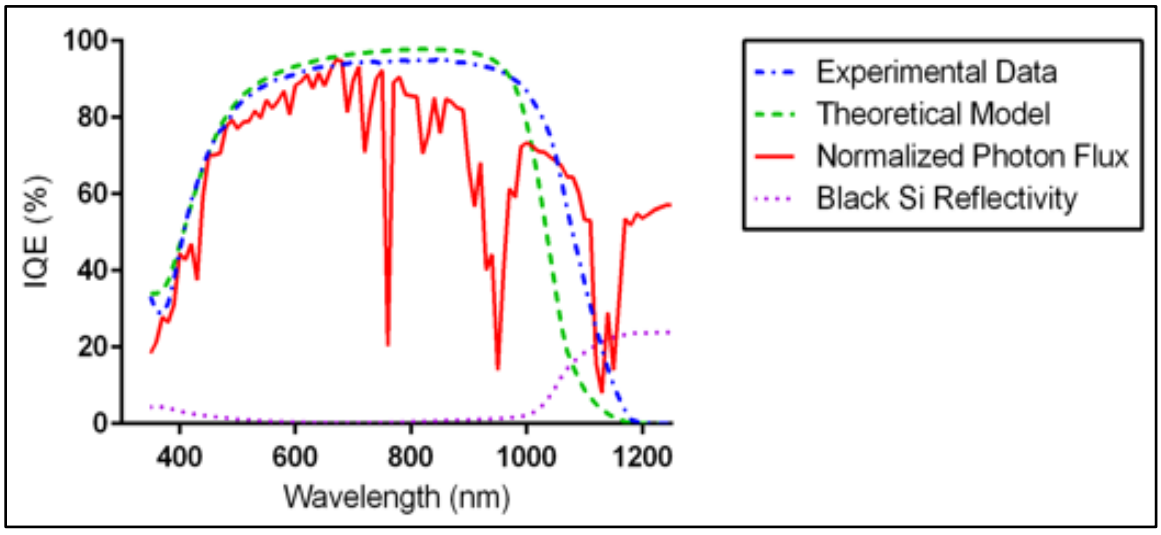

(b)

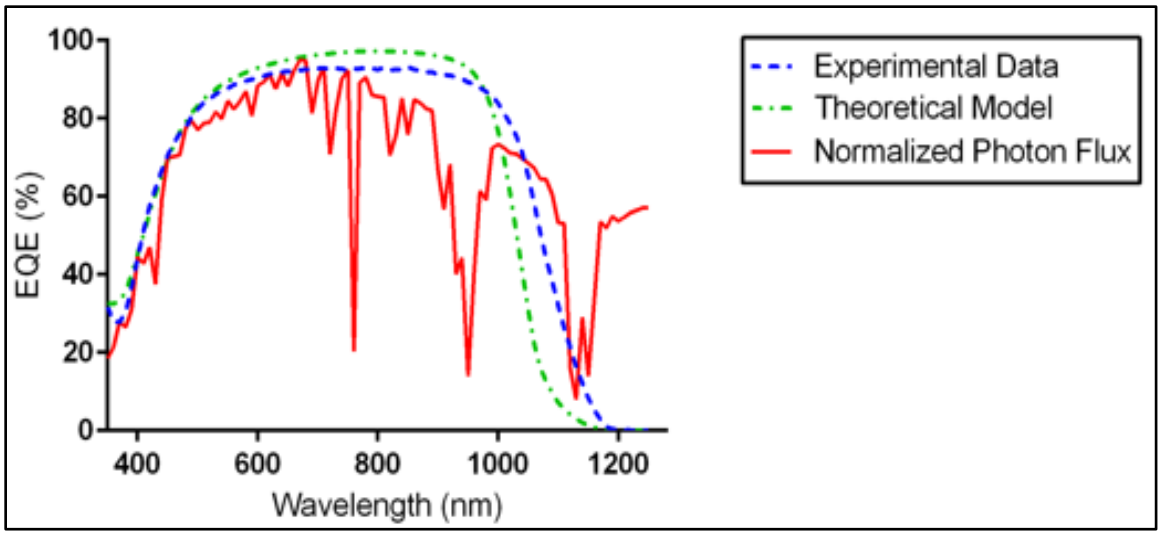

(c)

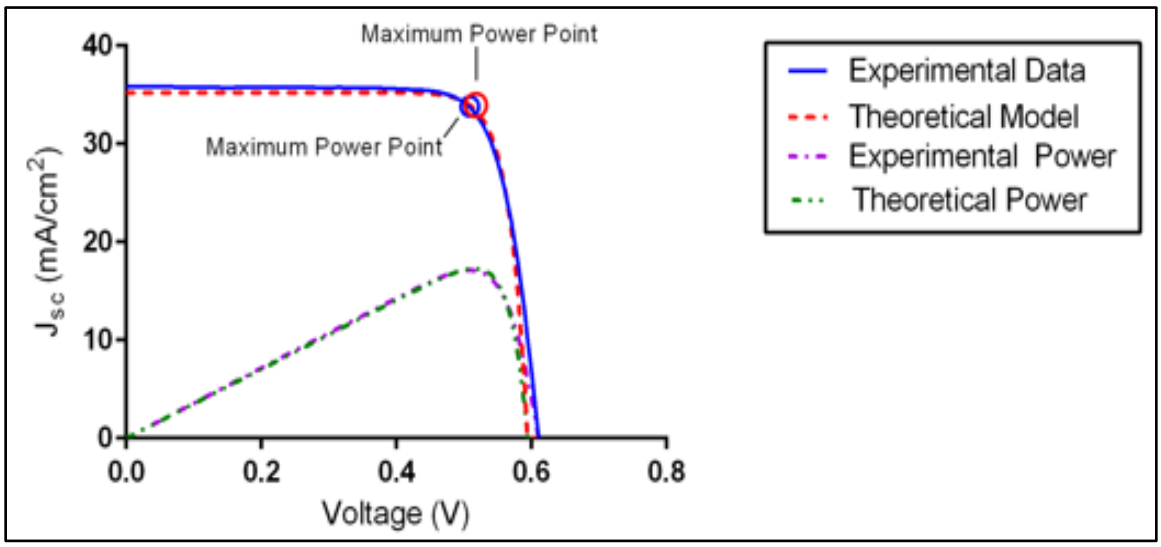

Figure 4. The (a) IQE, (b) EQE, and (c) IV curves of a single junction bSi solar cell. The theoretical data of the model was compared with an actual cell provided by Toor et al [4].

2. TANDEM JUNCTION SOLAR CELLS

2.1 Tandem Junction Cell Model

The tandem junction solar cell model was based on the same principles and set of equations as the single junction solar cell model, using the general structure found in *Figure 5*. The model allows a user to select a planar Si, SiN_x, or bSi bottom cell as well as a top cell of a different material. Our research focused on a perovskite top cell rather than other thin film materials, which is further discussed in the next section.

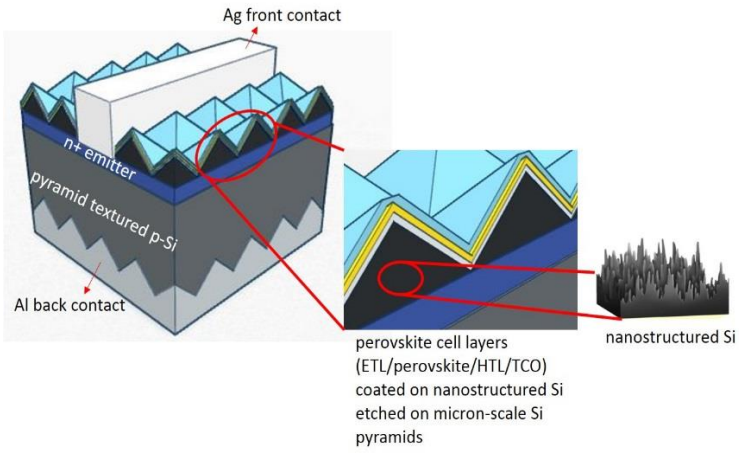

Figure 5. Schematic of proposed tandem junction cell consisting of a perovskite top cell and bSi bottom cell.

Along with the cell materials, the configuration of the tandem cell is also determined by the user. A series connected tandem cell or an n-terminal tandem cell can be modeled. A series connected tandem cell has a current-matching property, meaning that the photocurrent in the bottom cell must match the photocurrent in the top cell [10]. While series-connected cells are easier to manufacture, they result in lower efficiencies due to the current-matching property. In an n-terminal tandem cell, the two different solar cells are externally wired and have a coupling layer, which is shown in *Figure 6*.

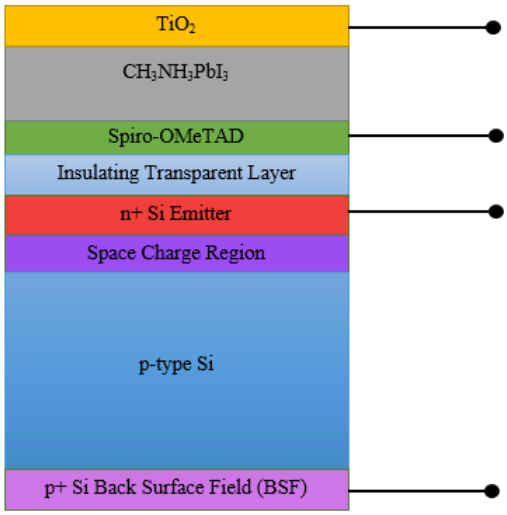

Figure 6. An n-terminal tandem cell configuration.

In this case, the photocurrents do not have to match, resulting in higher efficiencies. However, they are costlier to manufacture, and the coupling layer must be designed to provide optimal optical characteristics. In a tandem cell, the top cell is designed to absorb shorter wavelengths of light while the bottom cell is designed to absorb longer wavelengths of light. The bottom cell does not see any light that is absorbed by the top cell, which is accounted for by the model. The IQE and EQE of the cells are calculated separately in both configurations. For the n-terminal cell, the open circuit voltage and short circuit current are calculated for the bottom and top cell, and the total voltage or current is the sum of the two. The fill factor and efficiency are calculated similarly. For a series cell, the current is the same throughout, but the open circuit voltages of the cells are added to give the total voltage. The fill factor and efficiency are then calculated in the same manner as the n-terminal cell.

Once the input parameters for each of the materials of the tandem junction solar cell have been set and the configuration has been chosen, the model outputs the EQE, IQE, and IV curves of the individual cells as well as the tandem cell, showing the photon flux of the AM1.5G solar spectrum. It also outputs the voltage, current, efficiency, fill factor, and maximum power output for the individual cells and the tandem cell. The parameters of the cells can be optimized to theoretically give a high efficiency tandem cell greater than 30%.

2.2 Optimization of Perovskite and Silicon Solar Cell

There are many things to take into consideration when choosing a top cell material to be paired with a Si bottom cell in a tandem configuration, one of which is band gap. Si has a band gap energy of 1.12 eV and has high absorption in the 600-800nm range. Therefore, the optimal material bandgap to be paired with Si is about 1.8 eV, since the tandem cell will see high absorption across the entire solar spectrum, rather than a small range of wavelengths. One such material with a larger bandgap than Si is the perovskite. Perovskites have been researched since 2009 [11] for use in thin-film solar cells. Starting at a 4% efficient cell, perovskites have shown rapid progress demonstrating a 10.9% efficient cell mid-2012 improving as high as 17.9% in 2014 [12]. Perovskites are materials following the formula ABX_3 where A and B are cations of different sizes, and X is an anion [13]. In this thesis, A is the organic cation methylammonium (MA) ($CH_3NH_3^+$); B is the inorganic cation lead (Pb); and X is a halide anion, which can be based upon iodide (I^-), a mixed iodide and bromide ($I_{3-x}Br_x$), or iodide and chloride ($I_{3-x}Cl_x$). A schematic of the molecular structure of perovskite is shown in *Figure 7*.

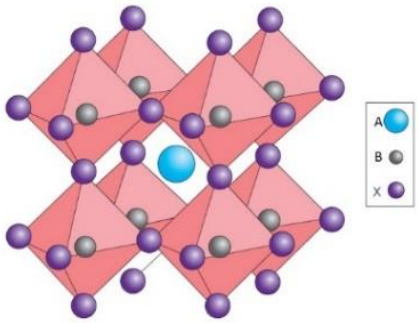

Figure 7. The molecular structure of perovskite. Reprinted by permission from Nature Publishing Group: Nature Materials 13, 838-842 (2014) License number: 3852560435429.

Perovskites have a tunable bandgap of 1.5-2.2 eV, making them a versatile top material to be paired with Si in a tandem cell. The absorber's bandgap enables the

necessary optical properties and longer diffusion lengths, allowing for higher efficiencies. A parametric study was conducted where the bandgap and thickness of the perovskite absorber ($CH_3NH_3PbI_3$) were varied, and the corresponding efficiencies were recorded. The thickness of the perovskite layer ranged from 50nm to 700nm, and the bandgap was changed from 1.5 eV to 2.2 eV. The generated contour plots are shown in *Figure 8* below for a bare Si bottom cell, SiN_x coated bottom cell, and a bSi bottom cell.

(a)

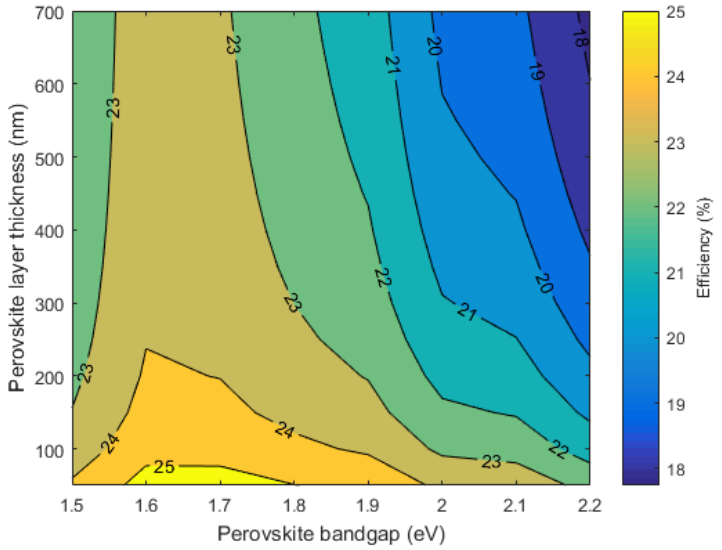

(b)

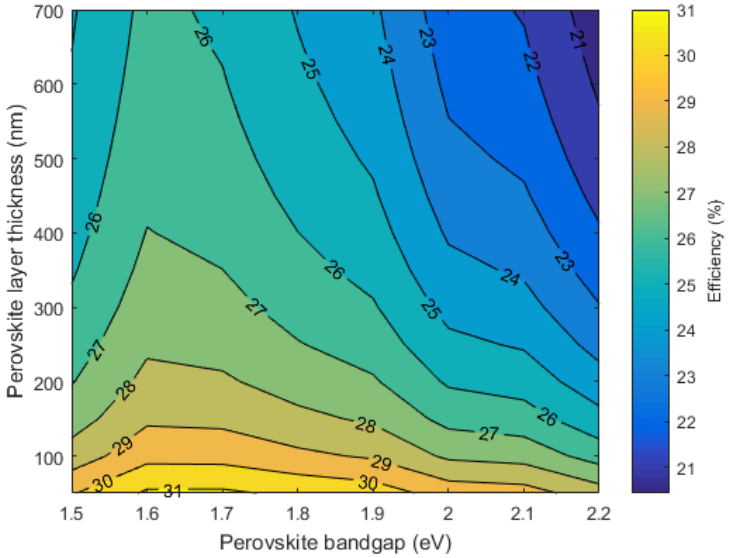

(c)

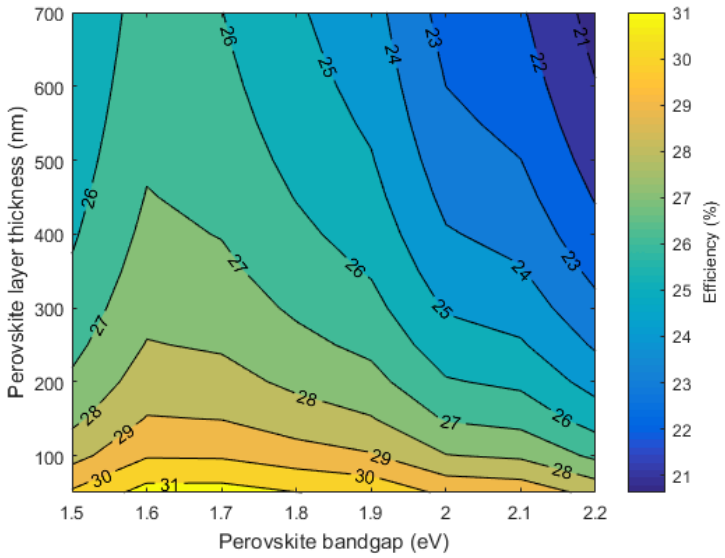

Figure 8. N-terminal tandem cell efficiency contour plot with respect to perovskite cell thickness for (a) bare Si, (b) Si with SiN_x AR coating, and (c) bSi.

From the contour plots, the highest range of efficiencies relative to any absorber thickness is reached at a bandgap of approximately 1.65 eV. With a bandgap of 1.57 eV, the lead-based perovskite's ($CH_3NH_3PbI_3$) chemical formula can be altered to include chlorine ($CH_3NH_3PbI_{3x}Cl_x$). The mixed-halide perovskite then has a bandgap of 1.6 eV, exhibiting better environmental stability and carrier transport with diffusion lengths of up to 1.9µm for electrons and 1.2µm for holes than its pure iodide equivalent, which has a carrier diffusion length of approximately 100nm. By adjusting the chemical makeup of the absorber, the bandgap and diffusion properties are optimized, resulting in higher efficiencies. Similarly, the Si bottom cell can be optimized, resulting in the tandem cell efficiencies of greater than 30%.

A tandem junction cell comprised of the thin-film, lead-based perovskite top cell and a wafer-based Si bottom cell was modeled. Keeping the parameters of the top cell the same, results for a bare Si bottom cell, SiN_x coated bottom cell, and bSi bottom cell are discussed further. The efficiency of the tandem cell can be optimized by adjusting the parameters of the bottom cell. A Si bottom cell with a SiN_x coating or a bSi bottom cell result in a higher tandem cell efficiency than the planar Si bottom cell. The nanostructure

of the bSi cell and the SiN_x coating passivate the Si surface, improving the efficiency of the bottom cell, thus improving the efficiency of the tandem cell. A parametric study was conducted, modeling the change in efficiency as a function of the perovskite absorber thickness for a planar Si cell, a SiN_x coated cell, and a bSi cell. *Figure 9* shows the results of this study.

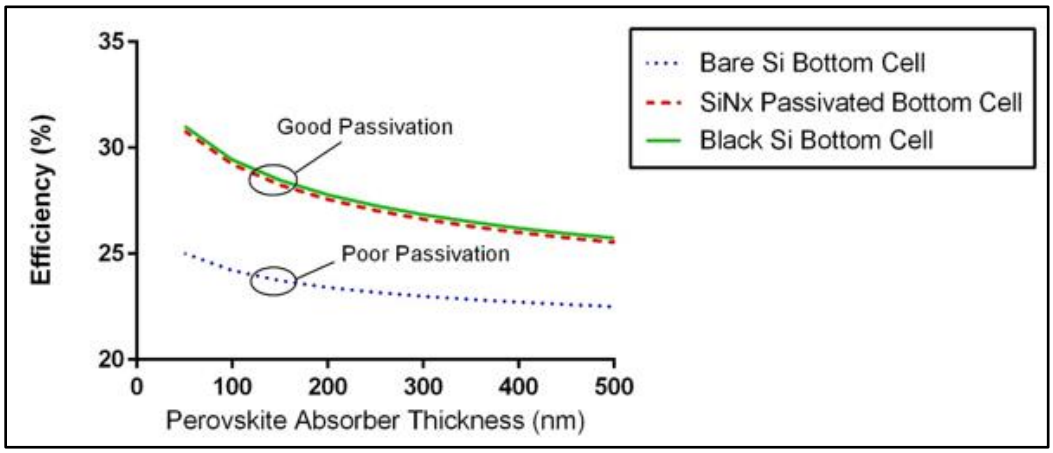

Figure 9. Parametric study of the n-terminal tandem cell efficiency with respect to the perovskite top cell thickness. The black Si bottom cell shows the highest efficiency profile.

The above figure shows that while the bSi cell and SiN_x coated cell result in a much higher efficiency than the planar cell, due to good surface passivation, the bSi cell results in the highest efficiency profile for the tandem junction solar cell. A tandem cell consisting of a bSi bottom cell and a perovskite top cell in the n-terminal configuration was modeled. The IQE, EQE, and IV curves for the cell that resulted in a 31.78% efficiency are shown in *Figure 10*.

(a)

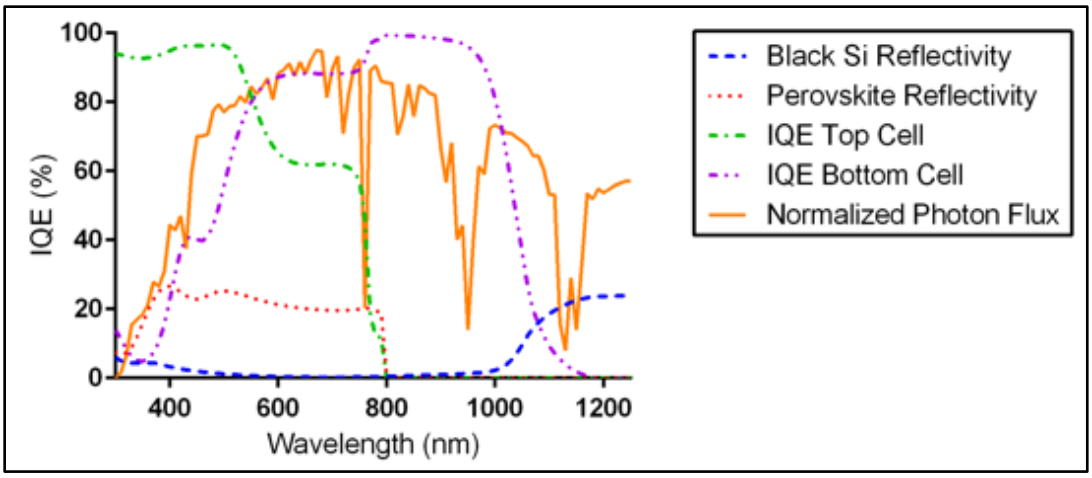

(b)

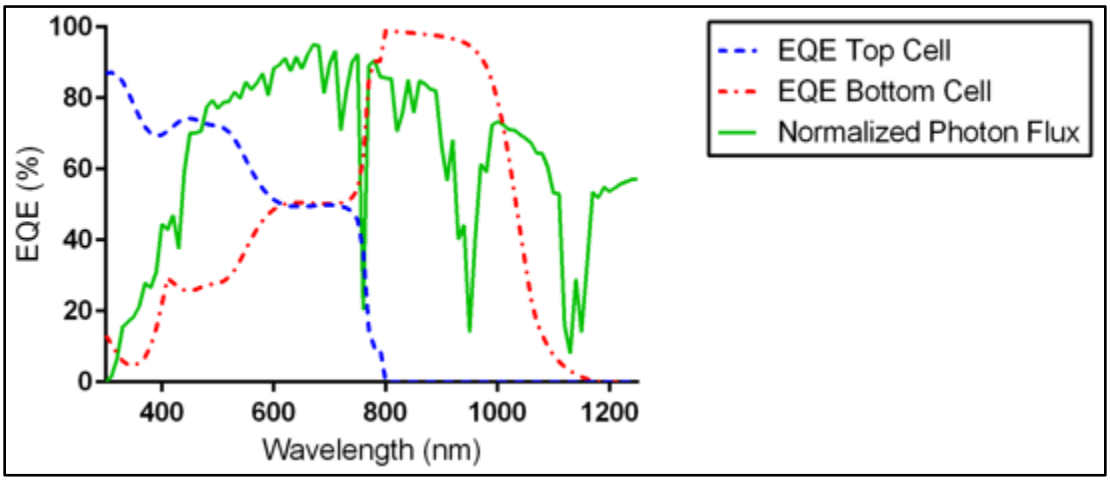

(c)

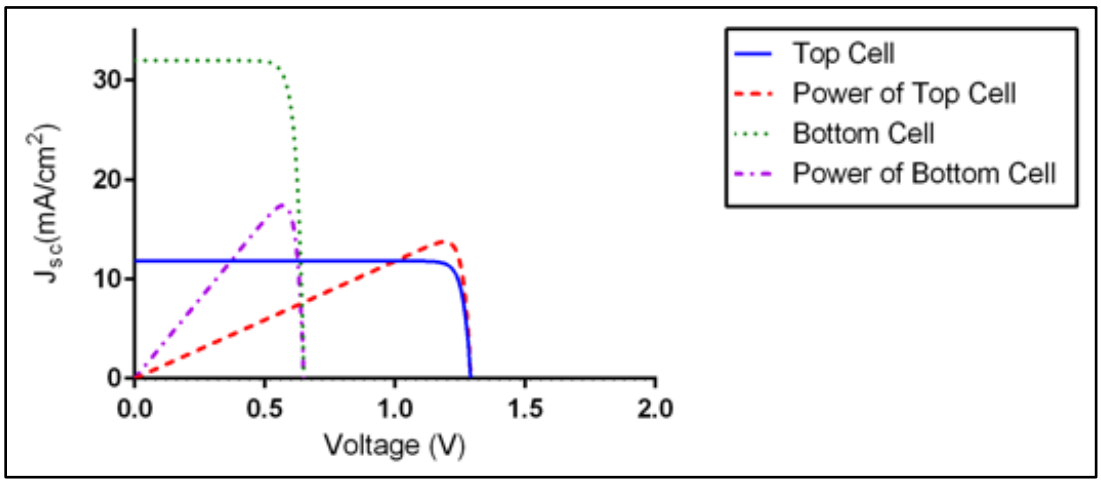

Figure 10. The (a) IQE, (b) EQE, and (c) IV curves of an n-terminal tandem cell with a bSi bottom cell. The overall efficiency for the cell was 31.78%.

3. SURFACE PASSIVATION TECHNIQUES

3.1 Anti-Reflection Techniques

One technique in improving the performance of solar cells is to incorporate an anti-reflective coating. By reducing the reflectivity of the surface—specifically at the range of wavelengths where the photon flux is maximized—more photons are absorbed, increasing the current density and efficiency of the cell. Reduced surface reflectivity can be accomplished with a deposited film, such as silicon nitride (SiN_x) or silicon dioxide (SiO_2), or by texturing the surface of the substrate. Most high efficiency Si cells use a combination of surface texturing and film coating to improve the reflectivity of the surface and to improve the surface passivation of the cell [14-16]. There are many different techniques in obtaining a textured surface; however, chemical etching is a very common low-cost option. By using different solutions, a range of surface structures can be etched: pyramids, inverted pyramids, nanorods, nanoporous surface, etc.

A pyramid structure, with structure sizes in the micron range, is the result of a potassium hydroxide (KOH) etchant, and reduces the surface reflectivity significantly compared to planar silicon. However, the average reflectivity of the surface can be reduced to less than 5% by creating a nanostructure, with structure sizes in the nanometer range. Nanorods or a nanoporous structure can be obtained by a metal-assisted chemical etching (MACE) process [4-7], involving two different solutions: the first to deposit metal particles, often silver (Ag), on the surface and the second to etch the particles into the Si substrate, creating the nanostructure. The metal particles are then removed by ultrasonication. The resulting surface looks black, thus the name black Silicon (bSi). *Figure 11* shows the reflection data of porous bSi compared to the reflection data of a planar Si substrate with no surface texturing or anti-reflective coating. The absolute reflectivity is reduced by approximately 35%. While the surface reflection is significantly reduced, the nanostructure degrades the blue light response of the cell [4]. It is for this reason that a SiN_x film is desired for Si solar cells, since it reduces surface reflection and passivates the surface, leading to better front response and improved performance.

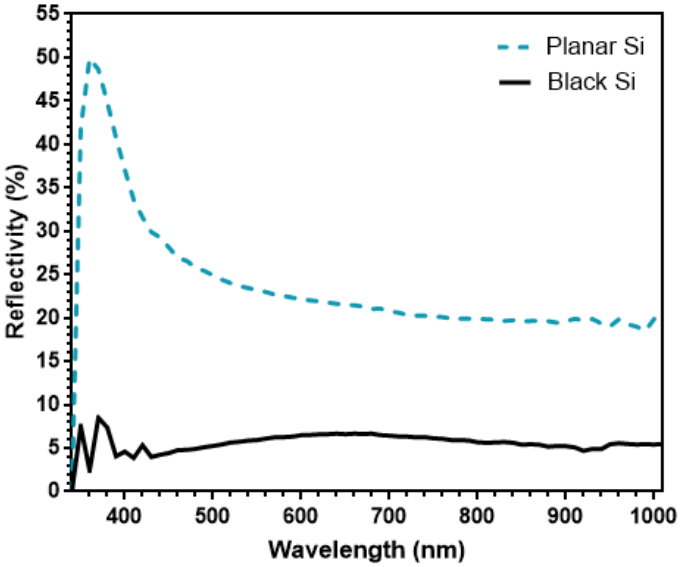

Figure 11. Reflection data of planar Si with no surface texturing compared to nanoporous bSi.

3.2 Deposition of Silicon Nitride Anti-Reflection Coatings

Silicon nitride (SiN_x) was deposited on p-type Si substrates using a physical vapor deposition system, the Intlvac sputtering tool. Electrons, introduced through the non-reactive argon (Ar) gas, bombard the Si target, releasing Si particles. Nitrogen (N_2) is introduced into the vacuum chamber and reacts with the Si particles to form SiN_x, which coats the Si substrate attached to a plate in the system. The coating can be optimized for optical performance by adjusting the refractive index of the SiN_x as well as the layer thickness. The layer thickness is determined by the deposition rate and deposition time, while the refractive index is determined from the N_2/Ar gas flow ratio. A lower ratio, meaning less N_2 gas with an increased amount of Si particles, results in a higher refractive index. A higher N_2/Ar ratio results in a lower refractive index as there are less Si particles in the system.

Literature has characterized this relationship extensively for films deposited using Plasma-Enhanced Chemical Vapor Deposition (PECVD) [14-16], where the SiN_x coatings have refractive indices that range from 1.9-2.3 [15]. PECVD coatings are a standard of the solar cell industry for their role as both an anti-reflection coating and

surface passivating layer. However, these systems often use Silane (SiH_4) and Ammonia (NH_3), both of which are highly toxic gases, in order to create the SiN_x layers. By using the sputtering tool instead, a SiN_x layer with the same anti-reflection and surface passivating properties can be realized without the use of toxic gases [17]. A larger range of refractive indices can also be reached by changing the argon and nitrogen gas ratio.

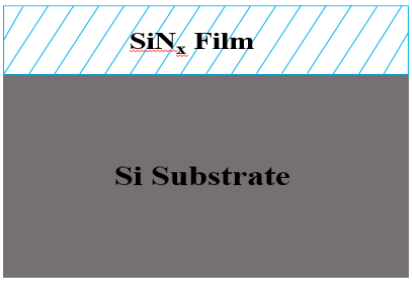

Figure 12. Structure of SAR SiN_x film of Si substrate.

For a single layer of SiN_x on a Si substrate as shown in *Figure 12*, the refractive index and layer thickness were determined by the equations below. The refractive index of the SiN_x layer is optically optimized by equation (3.2.1) [18], where n_0 is the refractive index of air or 1, and n_2 is the refractive index of silicon or 3.42. This gives an optimum value of 1.85 for the refractive index of SiN_x.

$$n_1 = \sqrt{n_0 n_2} \tag{3.2.1}$$

The optimum thickness of the layer is dependent upon the refractive index and the desired wavelength for reduced reflectivity. This wavelength was set to 600nm, which is within the range of wavelengths where the solar flux is maximized. This ensures that the solar cell has the lowest reflectivity where the highest number of photons are available. The thickness is then determined by equation (3.2.2). Using the values of $\lambda = 600nm$ and $n_1 = 1.85$, the optimum thickness is 81nm.

$$t_1 = \frac{\lambda_0}{4n_1} \tag{3.2.2}$$

The reflectivity of the sample, based upon the refractive index, thickness of layer, and target wavelength, is determined by equation (3.2.3) [18]

$$R = |r^2| = \frac{r_1^2 + r_2^2 + 2r_1 r_2 \cos(2\theta)}{1 + r_1^2 r_2^2 + 2r_1 r_2 \cos(2\theta)} \tag{3.2.3}$$

where,

$$r_1 = \frac{n_0 - n_1}{n_0 + n_1} \tag{3.2.4}$$

$$r_2 = \frac{n_1 - n_2}{n_1 + n_2} \tag{3.2.5}$$

$$\theta = \frac{2\pi n_1 t_1}{\lambda} \tag{3.2.6}$$

A study was then conducted to determine the range of refractive indices of the SiN_x layer that could be obtained by adjusting the gas flow ratios [15]. The sputterer had an average deposition rate of 10.25 nm/minute, and the flow rate of argon (Ar) was set to a constant flow rate of 8sccm, while the nitrogen (N_2) gas flow rate was varied from .8sccm to 14sccm for a total deposition time of 6 minutes. The flow rates, gas ratios, and corresponding refractive indices are shown in the *Table 3* and *Figure 13* along with the average reflection values for the SiN_x layer. The refractive index and the thickness of the layer were measured using an ellipsometer. The figure and table show that the reachable refractive indices for SiN_x range from approximately 1.65 to 2.60. A one-phase exponential decay was fitted to the data so that the gas flow rate could be calculated easily for a desired refractive index.

Table 3. Refractive indices and average reflection data for various SiNx films for increasing gas ratios.

Gas flow rate of N_2 (sccm)	Ratio of N_2:Ar	Refractive Index of SiN_x	Layer Thickness (nm)	R_{ave} (%)
.8	.1	2.612	88.75	15.06
2	.25	2.327	70.06	7.71
4	.5	1.936	67.13	6.70
6	.75	1.771	65.65	7.42
8	1.0	1.699	63.51	8.75
10	1.25	1.736	59.69	8.43
12	1.50	1.647	63.72	9.35
14	1.75	1.687	59.31	9.67

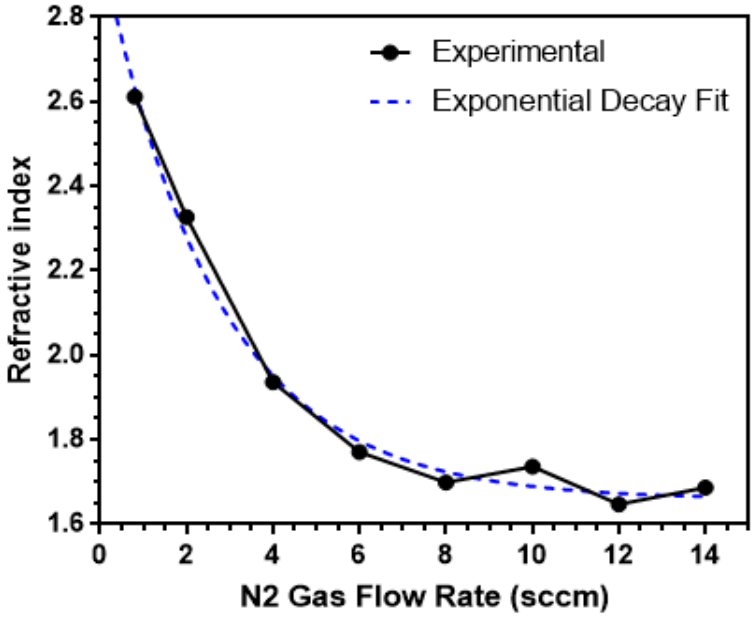

Figure 13. Graphical representation of the data given in *Table 3*, fitted with a one-phase exponential decay function.

The reflection data for the SiN_x samples is given in *Figure 14*. While most of the curves show the lowest reflectivity in the 400-500nm range (see equation (3.2.2)), the samples with .8sccm and 2sccm of N_2 have significantly different curves. This is due to

the increased thickness of the layers so that the reflectivity minima are at the wavelengths of 927nm and 652nm respectively, which can be seen in the reflection data. The increase in thickness can be attributed to an increase in the deposition rate when little nitrogen is present in the system.

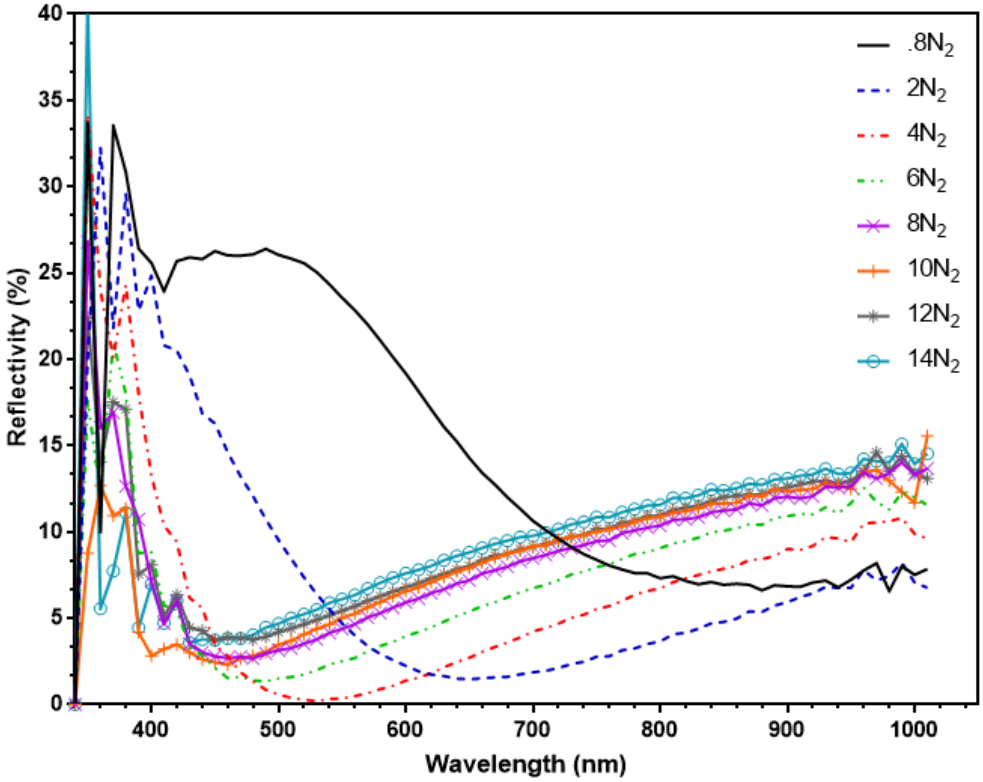

Figure 14. Reflection data for the SiN_x films at varying gas ratios.

3.3 Silicon Nitride Double Anti-Reflection Coatings

Single layer SiN_x films are an industry standard component of solar cell manufacturing as they passivate the surface of the cell and decrease the reflectivity, enhancing the overall performance of the solar cell. However, double anti-reflection (DAR) coatings have also been investigated for their increased reduction of the reflectivity of the surface, enhancing the efficiency of the cell even more [19]. Du et al [20] showed a greater improvement in V_{oc} and J_{sc} with a double anti-reflective coating of SiN_x compared to a single anti-reflective coating of SiN_x. The bottom layer of the double

anti-reflective coating better passivates the surface of the cell due to its larger refractive index [20], while the top layer aids in reducing the surface reflectivity of the cell. A Matlab model was created in order to optimize the thickness and refractive index of the DAR SiN_x coating. The model is based upon *Figure 15* below, where the bottom layer that contacts the Si substrate has a higher refractive index than the top layer.

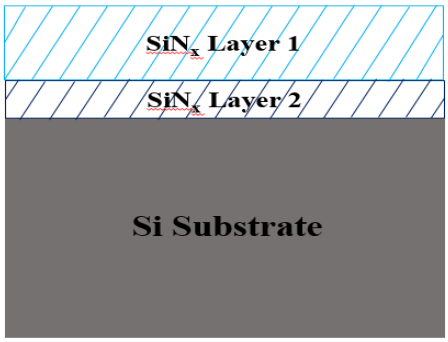

Figure 15. Structure of DAR SiN_x film.

The reflectivity is calculated using equation (3.3.1) [18],

(3.3.1)

$$R = |r^2|$$
$$= \frac{r_1^2 + r_2^2 + r_3^2 + r_1^2 r_2^2 r_3^2 + 2r_1 r_2(1 + r_3^2)\cos(2\theta_1) + 2r_2 r_3(1 + r_1^2)\cos(2\theta_2) + 2r_1 r_3 \cos\big(2(\theta_1 + \theta_2)\big) + 2r_1 r_2^2 r_3 \cos(2(\theta_1 - \theta_2))}{1 + r_1^2 r_2^2 + r_1^2 r_3^2 + r_2^2 r_3^2 + 2r_1 r_2(1 + r_3^2)\cos(2\theta_1) + 2r_2 r_3(1 + r_1^2)\cos(2\theta_2) + 2r_1 r_3 \cos\big(2(\theta_1 + \theta_2)\big) + 2r_1 r_2^2 r_3 \cos(2(\theta_1 - \theta_2))}$$

where,

$$r_1 = \frac{n_0 - n_1}{n_0 + n_1} \tag{3.3.2}$$

$$r_2 = \frac{n_1 - n_2}{n_1 + n_2} \tag{3.3.3}$$

$$r_3 = \frac{n_2 - n_3}{n_2 + n_3} \tag{3.3.4}$$

$$\theta_1 = \frac{2\pi n_1 t_1}{\lambda} \tag{3.3.5}$$

$$\theta_2 = \frac{2\pi n_2 t_2}{\lambda} \tag{3.3.6}$$

The model takes in the reflectivity of planar silicon and the photon flux, both of which are dependent upon wavelength. The refractive indices for the top and bottom layer of SiN_x are also, while the thicknesses are varied from 20nm to 120nm. The reflection data is calculated for each thickness, and the result is plotted in the figure below. The x-axis is the top layer thickness in nanometers; the y-axis is the bottom layer thickness in nanometers; and the z-axis is the reflectivity percentage. The color map of the surface corresponds to the wavelength in nanometers.

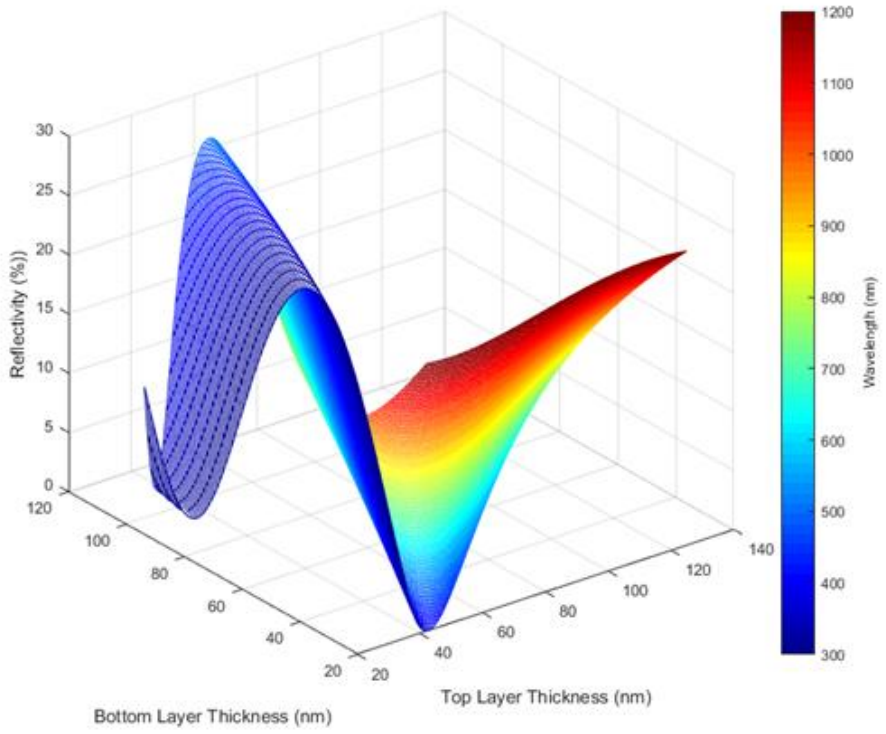

Figure 16. Contour plot of reflectivity as a function of film thicknesses for given refractive indices.

Since the photon flux is maximized at 500-700nm, the reflectivity should be minimized for this range. *Figure 17(a)* shows only the reflection dependence on the layer thicknesses for the range of 500-700nm, and *Figure 17(b)* shows the optimum bottom layer thickness.

a)

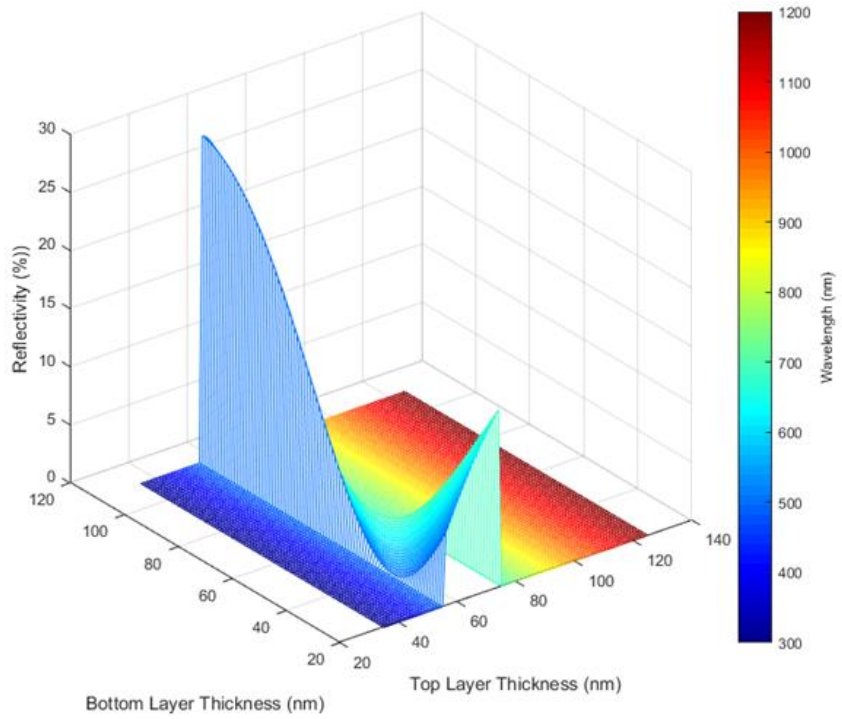

b)

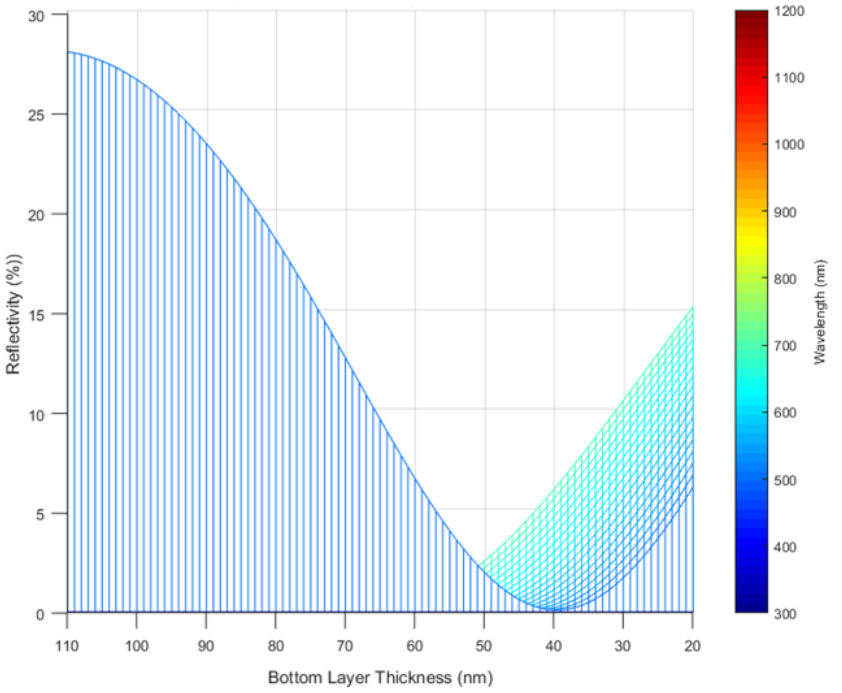

Figure 17. (a) Contour plot of *Figure 16* between the wavelengths of 500 and 700nm; (b) the reflectivity as a function of the bottom layer in the same range of wavelengths.

Once the bottom layer thickness has been determined, the Matlab model sweeps through multiple top layer thicknesses, creating a contour plot with the respective reflection values. For a top-layer refractive index of 1.9, a bottom layer refractive index of 2.0, and a bottom layer thickness of 30nm, the optimum top layer thickness is 35nm to 50nm, which is shown in *Figure 18*. Finally, by setting the value of the top layer thickness, the Matlab model gives the reflection curve of the DAR SiN_x film compared to the reflection curve of a planar Si substrate with no AR coating. The Matlab model also gives the spectrum-weighted average reflectivity values for each sample.

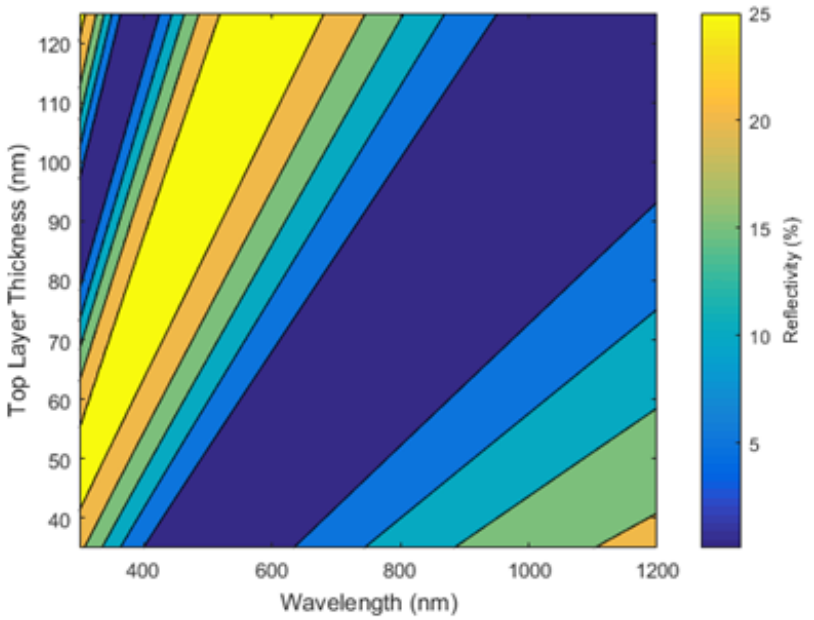

Figure 18. Contour plot of top layer thickness versus wavelength with a set bottom layer thickness. The reflectivity can be reduced to less than 5% for 500nm by setting the top layer thickness less than 50nm.

For a single AR coating on a Si substrate, the optimum refractive index is 1.85, found using equation (3.2.1). The film thickness of 81nm results in minimum reflection at a wavelength of 600nm, where the photon flux is at a maximum. Thus, the effective refractive index and thickness for the double AR coating should also be n = 1.85 and t = 81nm. This can be calculated using equation (3.3.7) below, where n_{SAR} is the refractive

index of the single AR coating and the quantity t_1+t_2 is the optimum thickness of the single AR coating.

$$n_{SAR} = \frac{n_1 t_1 + n_2 t_2}{t_1 + t_2} \tag{3.3.7}$$

For a Si solar cell not encapsulated by glass, the optimum refractive index of the bottom layer is 2.0 [20]. From the Matlab DAR model with a bottom refractive index of 2.0, the optimum thickness where the reflection is minimized is 30nm. Thus, n2 = 2.0, t2 = 30nm, and t1 = 50nm in order to optimize the total thickness at 80nm. Solving for the refractive index of the top SiNx layer, the DAR coating has a reflection minimum at 550nm when n1 = 1.75. The reflection curve using the parameters listed above is given by *Figure 19*.

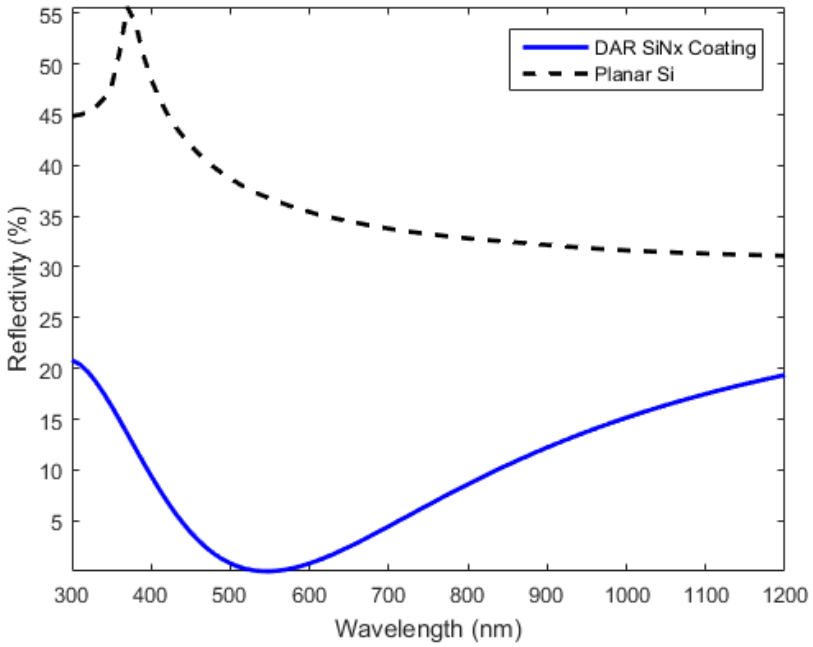

Figure 19. Reflection curve of DAR SiN_x coating with a top layer n = 1.75 and t = 50nm and a bottom layer n = 2.0 and t = 30nm.

4. FABRICATION OF SOLAR CELLS WITH IMPROVED FRONT RESPONSE

4.1 Fabrication of Silicon Solar Cells

A batch of eight planar cells were fabricated per the process further outlined in this section. The cells are cleaned with a 10% hydrofluoric acid (HF) and 90% deionized (DI) water solution for 1 minute. The HF dip makes the Si surface hydrophobic, meaning that water does not adhere to the surface. The cells are placed in a 5-minute hydrogen peroxide (H_20_2) bath to improve the hydrophilicity of the surface, so that water would adhere to the surface. This is desirable, since the dopant used is a solution consisting of 15% ammonium dihydrogen phosphate (ADP) and 85% DI water [8]. The dopant is spin-coated on the Si cells, and then they are placed in a quartz, open-tube diffusion furnace at 950℃ for 90 minutes. After the diffusion step is complete, the cells are placed in a 5-minute HF clean to remove the phosphosilicate glass (PSG) that formed during diffusion [8]. Next 3μm of Al is deposited through electron beam evaporation, and then the cells are again placed in the furnace for 10 minutes at a temperature of 1,000℃. This annealing step creates the highly-doped back surface field (BSF), which increases the electric field in the cell. After the back contact is finished, the front contacts are patterned on the cell using photolithography. Using electron beam evaporation, titanium (Ti) and silver (Ag) are deposited onto the cell, creating the front contacts. Lastly, single and double SiN_x coatings are sputtered onto the cells, and the quantum efficiency, current-voltage, and reflection data are measured. The resulting Si solar cell is shown in *Figure 20*.

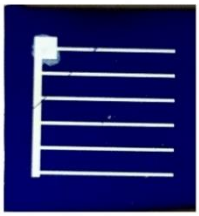

Figure 20. One of the fabricated Si solar cells with a DAR SiN_x coating. This particular cell had an efficiency of 7.49%.

4.1.1 Dopant

Phosphorous diffusion to form highly doped emitters is a very common process in the commercial production of silicon solar cells. Phosphorus oxychloride ($POCl_3$) is widely used for gaseous diffusion; however, it is a highly corrosive material [8] and a costly step. Instead, ammonium dihydrogen phosphate (ADP), which is a nontoxic material [8], was used as a doping source. ADP was dissolved in deionized (DI) water and deposited on the Si samples using the spin-coater. The spin speed and coating time was optimized for the desired range of sheet resistance values and will be discussed further in this section. After the solution was spin-coated on the sample, it was dried by placing the sample on a hot plate at 100°C for 8 minutes. The samples were then placed in an open quartz tube furnace at 950°C [8] for 90 minutes, shown in *Figure 21*. Before measuring the sheet resistance values, the samples were cleaned in an HF bath for 5 minutes removing the layer of PSG formed on the samples during the heating process.

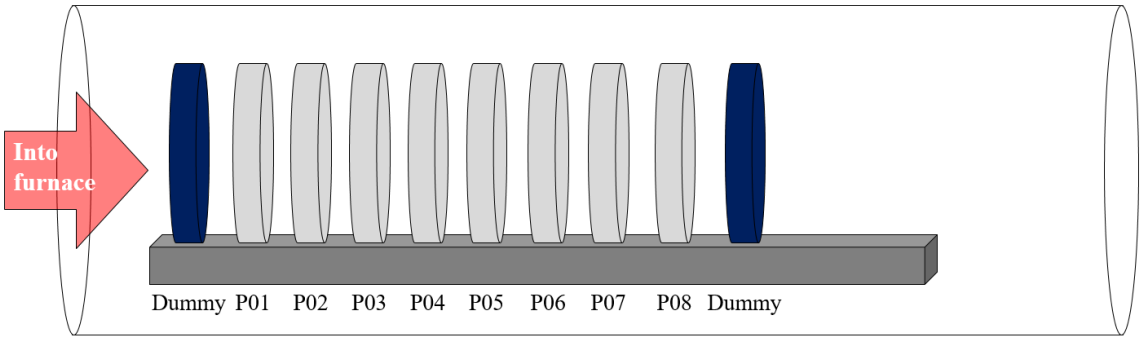

Figure 21. Solar cell placement in the open tube furnace. Dummy wafers were placed on the either ends of the wafer boat. Figure courtesy of Wenqi Duan.

The concentration of ADP, the spin speed, the ramp time, and the dwell time were all varied to find the parameters that gave the optimum sheet resistance values. For solar cells, the sheet resistance should range from 30-100 Ω/sq [21]; however, the optimum range is 50-70 Ω/sq. If the sheet resistance is too low, the carriers will recombine too quickly, and the current decreases, resulting in poorer performance. First, the ramp times

and dwell times at two different spin speeds were looked at. The ramp time is the time it takes for the spin coater to reach the desired speed, and the dwell time is how long the sample is spun at the desired speed. The ramp time was adjusted from 5s to 25s, and the dwell time was adjusted from 10s to 30s. Two separate batches were used: one at 10% (vol.) ADP concentration and the other at 5% ADP concentration. Half the samples in each batch were tested at 500rpm while the other half was tested at 1,000rpm. After measuring the sheet resistance at different places on the sample, it was noted that the samples spin-coated at 1,000rpm with a 15s ramp time and 30s dwell time were the most consistent in terms of sheet resistance across the entire sample, and the concentration was 10%.

For the next experiment, the concentration was 7% and 10%; the spin speed was 1,000rpm; the ramp time was 15s; and the dwell time was varied from 20s to 35s in increments of 5s. Again, the sheet resistance values were measured at different points of the sample to find which parameters gave the most consistent values across the sample. It was observed that the sheet resistance decreases as the volumetric concentration of ADP increases, and a 7% concentration gave sheet resistance values of 125-150 Ω/sq, which is greater than the optimum range. The ADP concentration affected the range of values reached, while the spin speed, ramp time, and dwell time affected the consistency of the values on the sample. The optimum parameters for this run were 10% ADP concentration, 1,000rpm spin speed, 15s ramp time, and 30s dwell time, giving a sheet resistance of 82.3Ω/sq.

The ADP concentration was increased to 15%, and the spin speed was changed to 2,000rpm, while the ramp time and dwell time were the same as above. After diffusion, the sheet resistance values were measured and recorded in the table below.

Table 4. Sheet resistance values of Si cells after doping with 15% ADP concentration.

Sample Number	Sheet Resistance (Ω/sq)
1	40.41
2	44.77
3	72.67

Table 4 continued.

4	64.10
5	63.19
6	58.60
7	89.50
8	17.90

The Si samples showed consistent sheet resistance values in the optimum range, with the exception of LD05_P8. The much lower sheet resistance value can be attributed to excess dopant on the surface after spin-coating the sample. Front contacts and back contacts were deposited onto the cells per the procedure defined in the following section.

4.1.2 Contacts

The back contacts of the cells are formed by depositing aluminum (Al) on the back side of the doped Si samples. Electron beam evaporation was used to uniformly deposit approximately 3μm of Al. Once the metal has been deposited, the samples go through an annealing step. The samples are placed in the open quartz tube furnace for 10 minutes at 1,000°C, so that the Al uniformly diffuses into the Si, creating the back-surface field (BSF). The highly doped BSF is an important component in the solar cell, because it collects carriers to the base, increasing the electric field in the cell and reducing rear-surface recombination [9]. Without the Al-BSF, the cell would have poor back response, resulting in lower efficiency. *Figure 22* shows a comparison of quantum efficiency curves of two cells with and without a BSF.

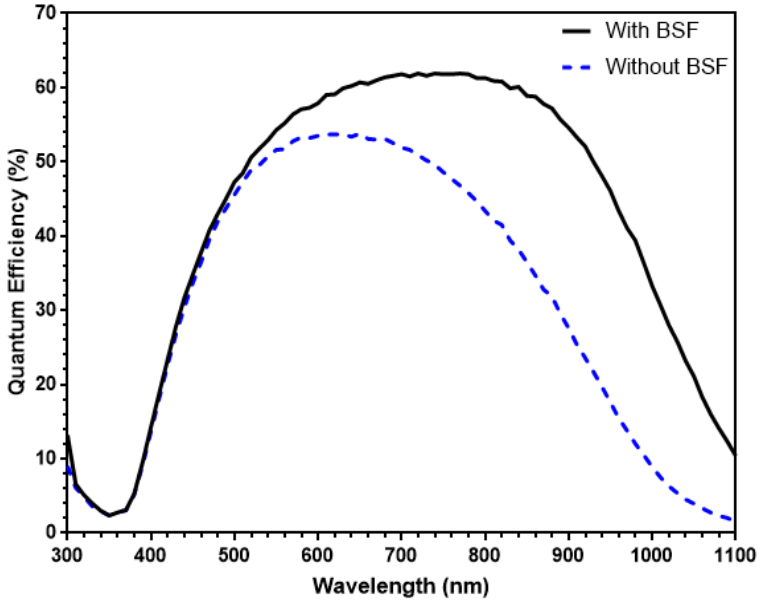

Figure 22. A cell with a back-surface field (BSF) has a much better rear response than one without, as shown by the external quantum efficiency (EQE) curves.

Once the back contacts and BSF have been formed, photoresist is painted on the back side. The cells are placed in an HF bath then in a developer containing alkalis, which would etch away at the metal contacts. The front contacts involve slightly more processing than the back contacts of the cell. After an HF clean, lift-off resist LOR-10B is spin-coated onto the front side of the cells, then dried by placing the cells on a hot-plate at 150°C for 3 minutes. A positive photoresist, AZ1518 is spin-coated on top of the LOR-10B and is dried by placing the cells on a hot-plate at 100°C for 4 minutes. The spin-coating parameters can be found below in *Table 5*.

Table 5. Photoresist spin-coating parameters.

Resist	Step #	Ramp Time (s)	Dwell Time (s)	Spin Speed (rpm)	Hot Plate Temperature (°C)	Hot Plate Time (min.)
LOR 10B	1	1	0	750	150	4
	2	10	30	3,000		
AZ1518	1	5	30	4,000	100	3

The lift-off resist is necessary because it reduces the time it takes to clean the remaining photoresist of the cells. AZ1518 is highly adhesive to Si, and the use of a lift-off layer reduces the clean time by hours. Using photolithography, the cells are exposed to light, per the contact pattern shown in *Figure 23* with 1x1cm area and 1.5mm finger spacing.

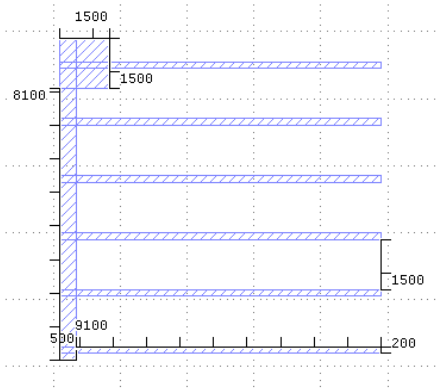

Figure 23. Front contact pattern with 1.5mm finger spacing.

After exposure, the cells are placed in two different AZ400K Developer baths, cleaning the softened photoresist from the contact pad area. Then the front contacts are formed by depositing 1μm of titanium/silver (Ti/Ag) using the electron beam evaporator. The cells are then placed in Remover PG to remove the remaining photoresist, cleaned with Acetone and IPA, and finally dried with an N_2 gun.

4.2 Surface Passivating Coatings

External quantum efficiency (EQE) and current-voltage (IV) measurements were taken for the six highest performing cells out of a total of eight cells. The sheet resistance, short circuit current density (J_{sc}), open circuit voltage (V_{oc}), fill factor (FF), and efficiency (η) for each cell are given in *Table 6*. The EQE curves are shown in *Figure 24(a)*, and the IV curves are shown in *Figure 24(b)*.

Table 6. Solar cell data of planar Si cells without SiN_x films.

Sample #	Sheet Resistance (Ω/sq)	I_{sc} (mA)	Cell Area (cm^2)	J_{sc} (mA/cm^2)	V_{oc} (V)	FF (%)	η (%)
LD05_P1	40.41	35.27	1.96	18.00	.5631	65.64	6.65
LD05_P2	44.77	32.67	1.885	17.33	.5533	70.33	6.74
LD05_P3	72.67	30.93	1.82	17.00	.5284	70.47	6.33
LD05_P4	64.10	31.49	1.96	16.07	.5305	70.80	6.03
LD05_P5	63.19	35.54	2.10	16.92	.5332	62.36	5.63
LD05_P8	17.9	32.57	2.175	14.97	.5536	66.19	5.49

(a)

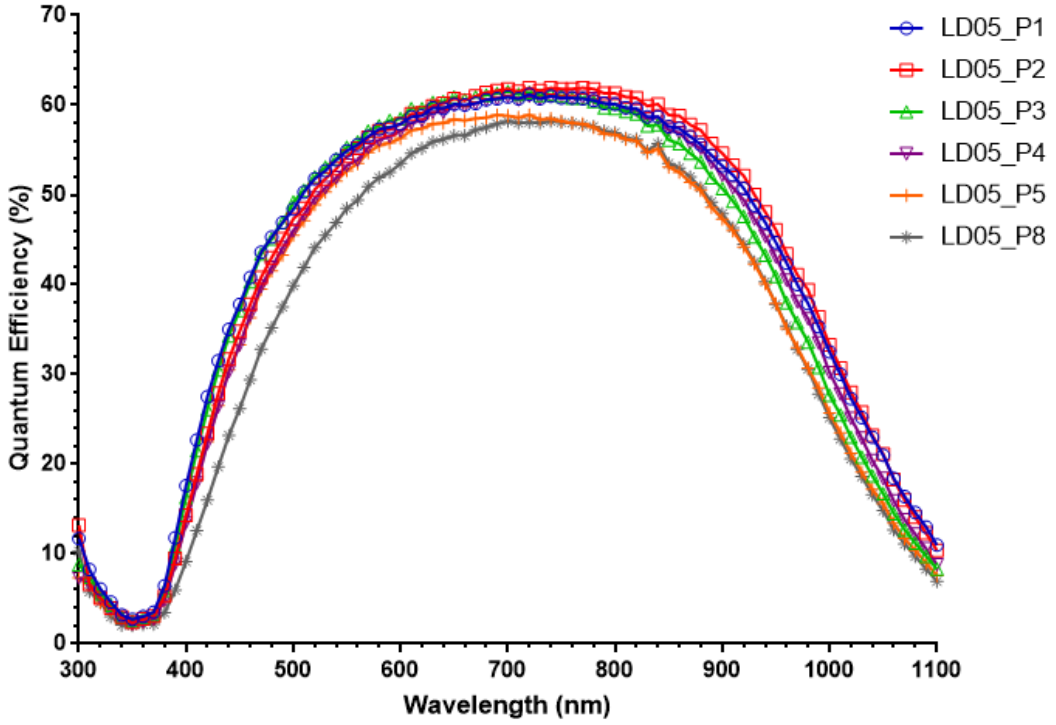

(b)

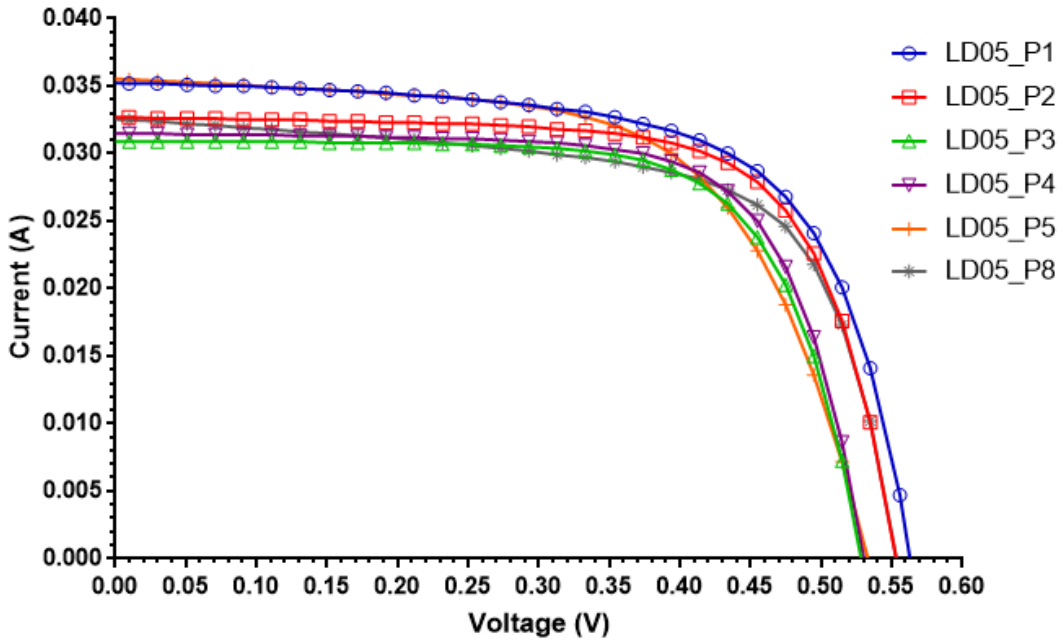

Figure 24. (a) The EQE curves of planar Si solar cells with no surface passivation, and (b) the IV curves of planar Si solar cells with no surface passivation.

Silicon nitride was sputtered on the cells given in the table above. Four of the cells had a double layer of SiN_x at varying refractive indices, and two of the cells had a single layer at two different refractive indices. For the double layers of SiN_x, literature reports that the best range of refractive index for the bottom layer is 2.0-2.3 [19, 20]. Therefore, two of the cells had a bottom layer with a refractive index of 2.0, and the other two cells had a bottom layer with a refractive index of 2.2. The top layers consisted of refractive indices of 1.7 and 1.9, while the single layer films had refractive indices of 1.7 and 1.9 also. The thicknesses of the double layer films were found from Du et al [20], and the single layer thicknesses were calculated using the equations given in Section 3.2. *Table 7* below shows the different layers, their refractive indices, thicknesses, and the gas flow rate of N_2 in the system to achieve the desired refractive index. The gas flow rates were determined using the data trend also found in Section 3.2.

Table 7. Gas flow ratios and desired thicknesses for DAR and SAR SiN_x films.

Sample #	n_1	n_2	gas flow rate for n_1 (sccm)	gas flow rate for n_2 (sccm)	thickness for n_1 (nm)	thickness for n_2 (nm)
LD05_P1	1.7	2.0	9.25	3.60	50.0	35.0
LD05_P2	1.7	2.2	9.25	2.37	50.0	35.0
LD05_P3	1.9	2.0	4.52	3.60	50.0	35.0
LD05_P4	1.9	2.2	4.52	2.37	50.0	35.0
LD05_P5	1.7	---	9.25	---	88.2	---
LD05_P8	1.9	---	4.52	---	79.0	---

After the films were deposited the EQE and IV curves were re-measured to see any improvement in response. The reflection data was also taken and internal quantum efficiency (IQE) curves were calculated. *Figure 25* shows the data with and without the SiN_x films as well as the IQE and reflection data. *Table 8* shows the performance data of the cells after the SiN_x layers were deposited.

Table 8. Solar cell data of planar Si cells with DAR and SAR SiN_x films.

Sample #	Sheet Resistance (Ω/sq)	I_{sc} (mA)	Cell Area (cm^2)	J_{sc} (mA/cm^2)	V_{oc} (V)	FF (%)	η (%)
LD05_P1	40.41	48.90	1.96	24.95	.5737	63.54	9.09
LD05_P2	44.77	44.24	1.885	23.47	.5623	69.24	9.14
LD05_P3	72.67	43.86	1.82	24.10	.5385	67.59	8.77
LD05_P4	64.10	42.77	1.96	21.82	.5397	68.54	8.07
LD05_P5	63.19	49.37	2.10	23.51	.5426	58.68	7.49
LD05_P8	17.9	44.72	2.175	20.56	.5637	67.90	7.87

a)

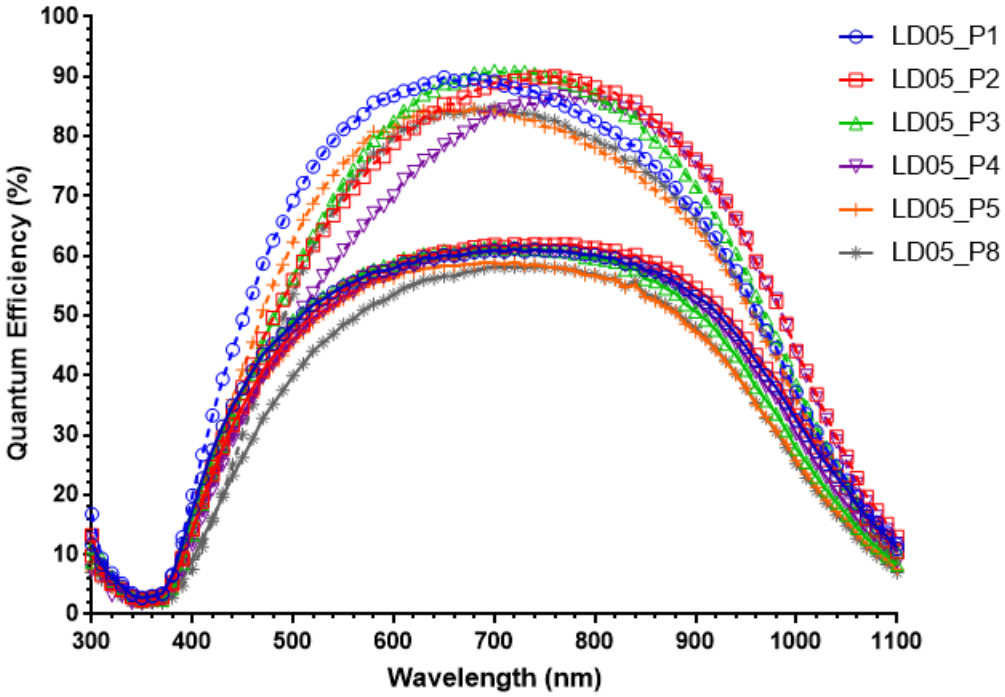

b)

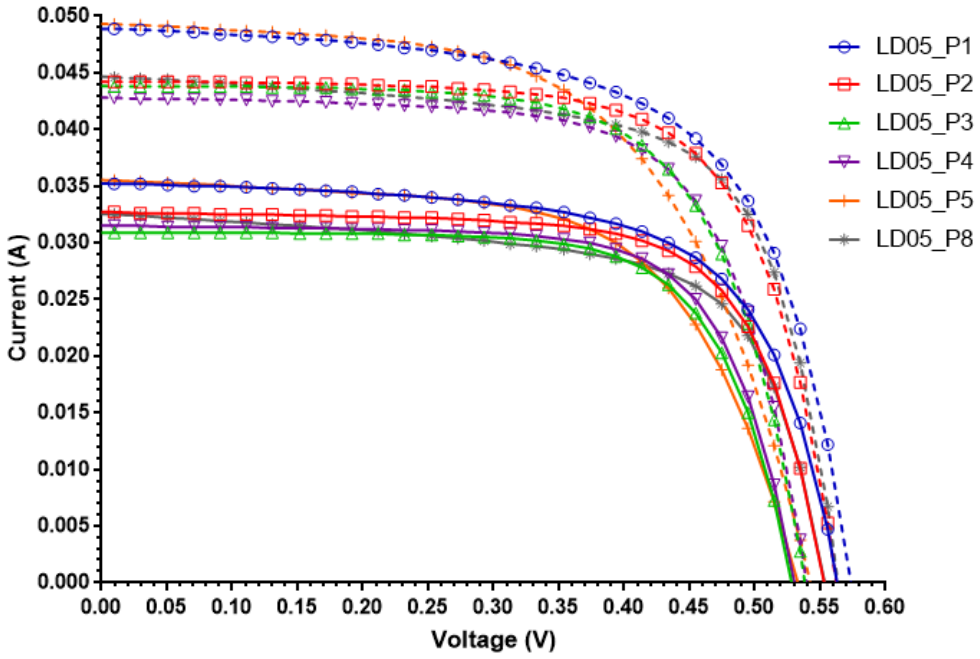

c)

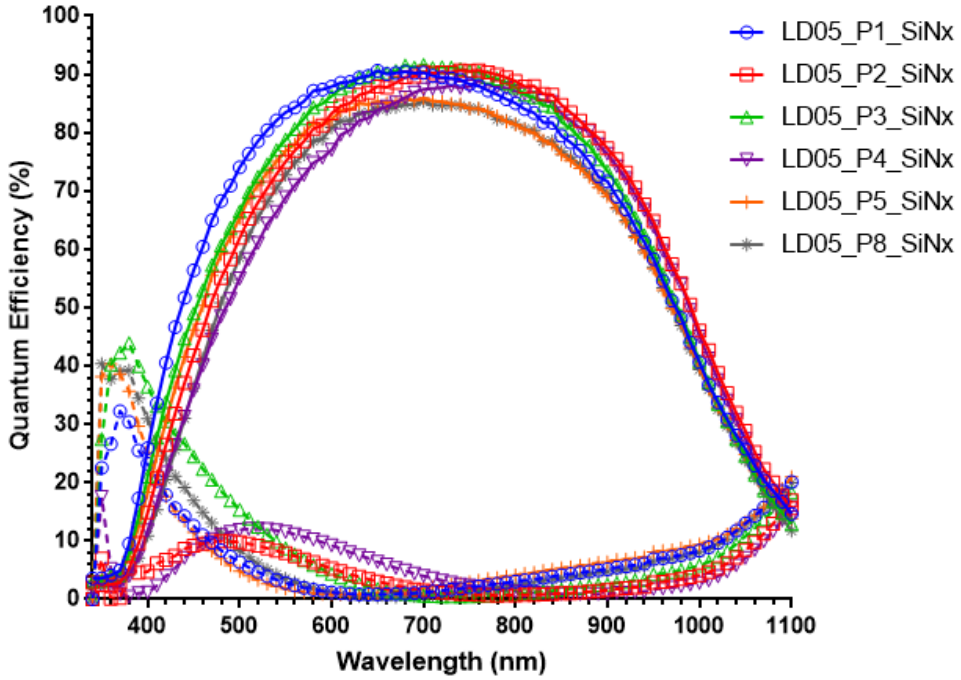

Figure 25. Comparison of (a) EQE, (b) IV, and (c) IQE and reflectivity curves with and without SiN_x films. The solid lines indicate the non-passivated cells, and the dashed lines indicate the cells with SiN_x films.

All the SiN_x films improved the performance significantly, resulting in up to a 1.8% absolute increase of efficiency and a 25.64% relative increase of efficiency. As the current and voltage of the cell increase, the fill factor decreases slightly—if the voltage and current do not increase by the same percentage. The increase in open circuit voltage indicates the surface passivation of the cell, confirming that the SiN_x films result in both decreased surface reflectivity and improved surface passivation. *Figure 26(a)* shows the absolute value changes in J_{sc}, V_{oc}, FF, and η, while *Figure 26(b)* shows the percentage change in the same variables.

a)

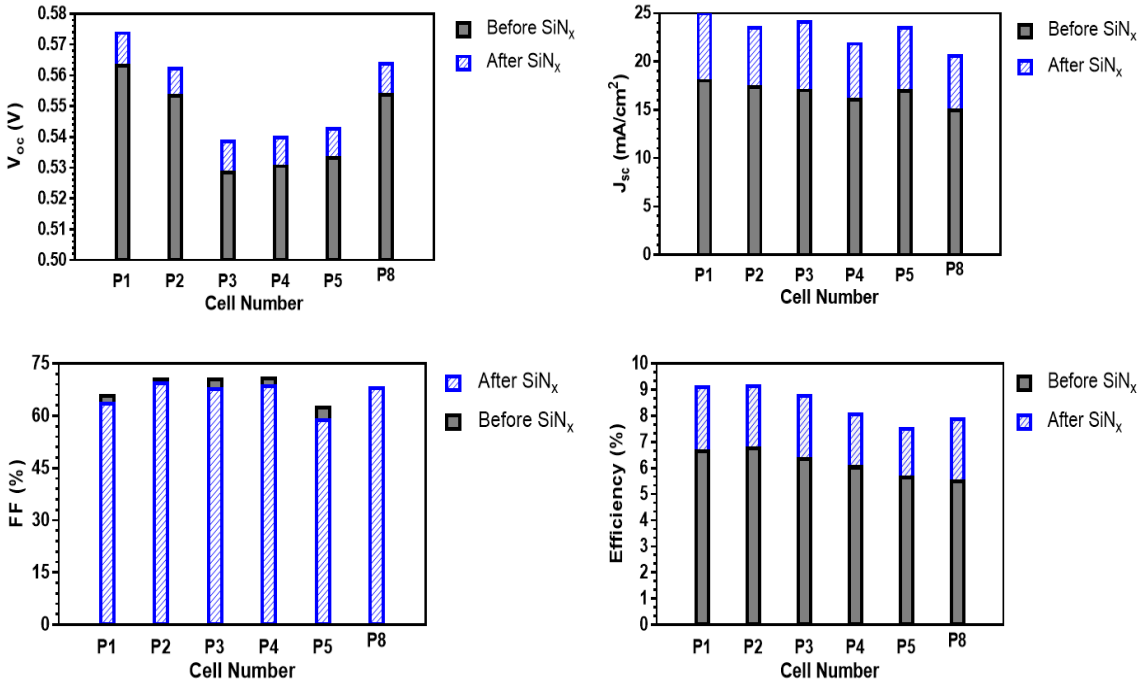

b)

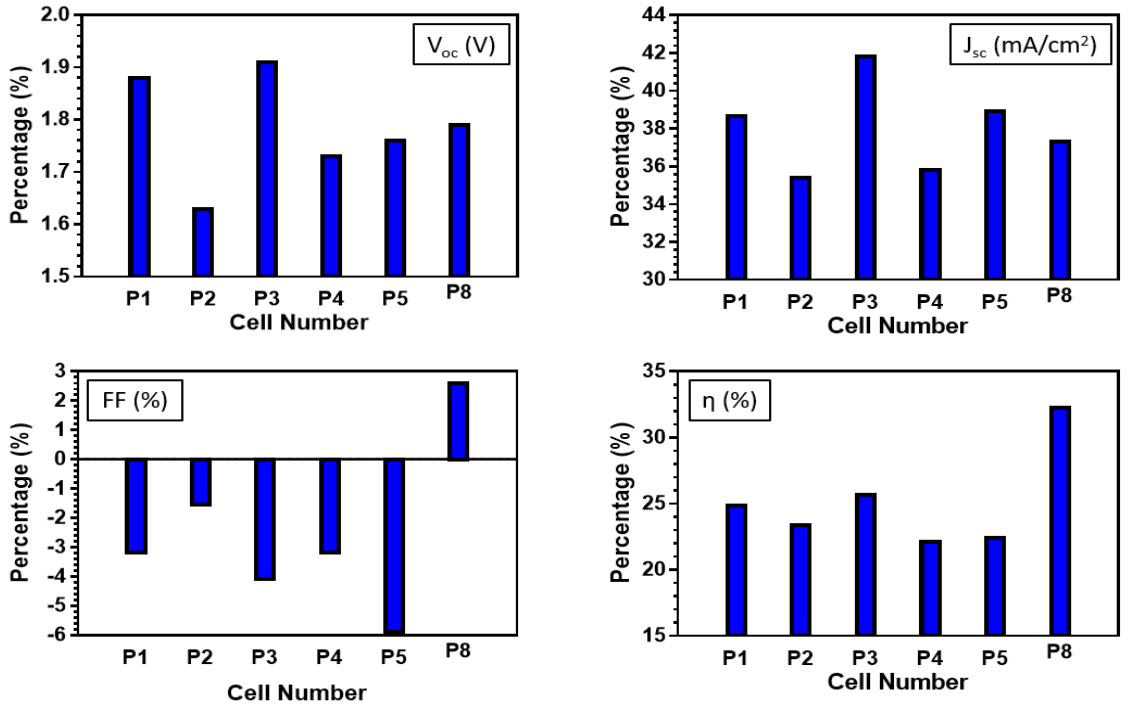

Figure 26. (a) The solar cell characteristic values before and after SiN_x was deposited and (b) the percentage change in values for the solar cell characteristic values.

While each film improved the performance of the cell, the film thicknesses were not optimized. Cell LD05_P3, which had a bottom layer refractive index of 2.0 and a top layer refractive index of 1.9, showed the most improvement; however, the thickness of the layers could be adjusted for better optical performance. The cell shows higher reflectivity where the solar flux is maximized, which is where the lowest surface reflectivity should be located at. By changing the layer thickness slightly, the reflection curve can be shifted so that the lowest reflectivity is seen at the 550nm wavelength. When the thickness of the bottom layer is changed to 30nm, and the thickness of the top layer is changed to 50nm, the minima shifts to 550nm. The reflection curve is given by *Figure 27*. By adjusting the thicknesses by a few nanometers, the cells can be optically optimized, resulting in higher efficiencies overall.

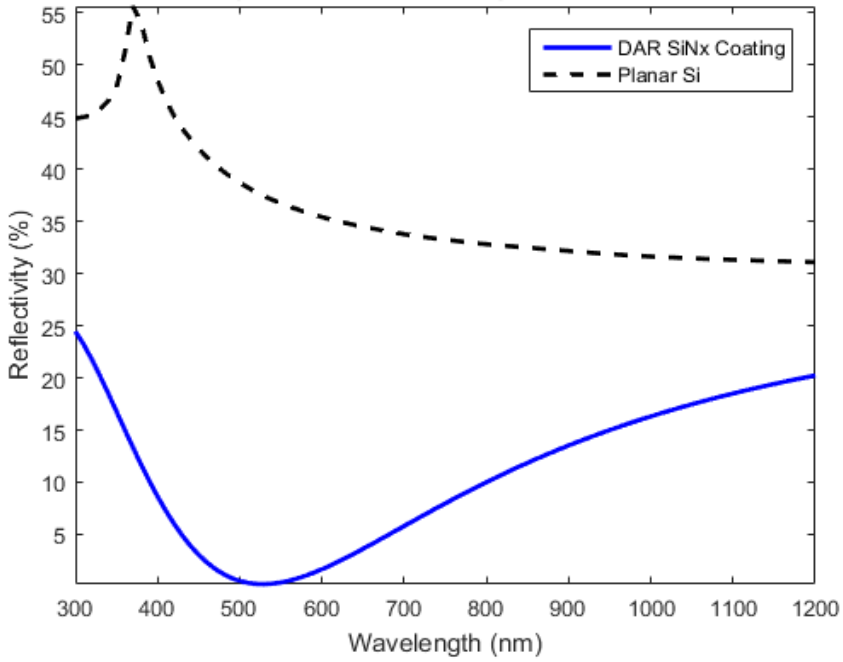

Figure 27. Reflection curve of DAR SiN_x coating with a top layer refractive index of n = 1.9 and a bottom layer refractive index of n = 2.0.

5. CONCLUSION

This thesis presented multiple techniques to achieve high efficiency solar cells, including tandem junction solar cells, nanostructured black silicon solar cells, and double layer anti-reflection coated solar cells. A tandem junction solar cell comprised of a perovskite top cell and silicon bottom cell was modeled. By optimizing the band gap energy of the perovskite top cell and using a nanostructured bSi bottom cell, an overall efficiency of 31.78% was reached.

The effects of a double layer anti-reflection SiN_x coating was further investigated. Silicon nitride films passivate the surface of the Si cells and reducing the surface reflectivity improving the open circuit voltage and short circuit current, respectively. By optimizing the refractive index and thickness of the film, the layer can significantly enhance the performance of the cell, greatly improving the efficiency. Single layer films were sputtered onto Si using different N_2/Ar gas ratios. Sputtering the films on, rather than using PECVD, results in the same enhancement of the cells without the use of toxic gases in the process. By adjusting the gas flow rate of nitrogen in the system, a range of refractive indices can be reached, varying from 1.65 to 2.60. The film refractive index is chosen so that the surface reflectivity is lowest at the wavelengths where the photon flux is maximized, which is 500-600nm; therefore, a SiN_x film with a refractive index of 1.85 was used.

A double anti-reflection SiN_x coating was modeled so that the mean refractive index was 1.85 and the thicknesses of the layers were optimized for the lowest reflectivity in the 500-600nm wavelengths. From the model, it was determined that the optimum film layers were as follows: the top layer had a refractive index of 1.75 at a thickness of 50nm, and the bottom layer had a refractive index of 2.0 at a thickness of 30nm.

Finally, planar Si solar cells were fabricated and double and single AR SiN_x films were sputtered onto the cells. Instead of the standard $POCl_3$ diffusion, a solution of ammonium dihydrogen phosphate (ADP) and DI water was spin-coated on the cells to create the n^+ emitter. Unlike $POCl_3$, ADP is not corrosive and is non-toxic, creating a cleaner and safer process, while still resulting in high fill factors and efficiencies. A 15%

concentration of ADP was spin-coated on the Si cells, which were then annealed in an open tube quartz furnace at 950°C for 90 minutes, giving sheet resistance values in the range of 45-75Ω/sq. Aluminum was then deposited onto the backside of the cells creating a back contact. The cells were then annealed in the furnace at 1,000°C for 10 minutes. The annealing step created the back-surface field (BSF), which improves the electric field in the cell, enhancing the back response of the cell. Using a photolithography step followed by a deposition of Ti/Ag, the front contacts are created.

The cells were measured before and after the sputtered SiN_x films, and the most improved cell had a V_{oc} = .5284 V, J_{sc} = 17.00 mA/cm^2, FF = 70.47%, and η = 6.33% before the DAR coating. After a DAR SiN_x film with a top layer thickness of 50nm and refractive index of 1.9 and a bottom layer thickness of 35nm and refractive index of 2.0, the V_{oc} = .5385 V, J_{sc} = 24.10 mA/cm^2, FF = 67.59%, and η = 8.77%. While the DAR coating increased the open circuit voltage, short circuit current, and efficiency of the cell, the film can be further optimized by adjusting the refractive indices and thicknesses of the layers. This work can be further expounded upon by studying the effects of DAR SiN_x coatings on bSi, which typically has poorer front response. Also, surface passivation films, such as aluminum oxide (Al_2O_3), deposited on the rear surface can be studied to improve the rear surface response of the cell, resulting in higher efficiency. Since silicon solar cells dominate the solar industry, the optimization of these cells through tandem structures or passivation films is crucial for the progress of low-cost, high efficiency solar cells.

APPENDIX

Matlab Code for Tandem Cell Model

```
% Author: Lauren Davidson
% Date: 6-25-15
% Description: This program models a Tandem Solar Cell comprised of
% Perovskite for the top cell and Silicon for the bottom cell. The user
can
% choose between an N-terminal device or a series device and can change
% parameters accordingly. The user is also able to load separate Excel
% files for different materials. The program uses the device
parameters,
% reflectivity, and absorption to calculate the power, efficiency,
voltage,
% and current of each cell as well as for the tandem cell. It then
displays
% the quantum efficiency curves, power curve, and IV curves.

clear;
close all;

%Define constants
q = 1.602e-19;  %Charge of electron (C)
h = 6.626e-34;  %Planck's constant
k = 1.3807e-23; %Boltzmann's constant
c = 299792458;  %Speed of light
n1 = 1;         %Refractive index of air
%Parameters of Top Material************************************
Nd1 = 3.17e20;      %Donor density (cm-3)
Dp1 = .43056;     %Hole diffusion coefficient in emitter (cm^/s)
tp1 = 16e-9;     %Hole life time in emitter (s)
Lp1 = 830e-7;   %Hole diffusion length in emitter (cm)
Na1 = 6.147e19;    %Acceptor density (cm-3)
Dn1 = .42025;        %Electron diffusion coefficient in base (cm^[1]/s)
tn1 = 16e-9;  %Electron life time in base (s)
Ln1 = 820e-7;     %Electron diffusion length in base (cm)
W1 = 100e-7;    %Thickness of Perovskite layer (cm)
Hpr1 = 200e-7;  %Thickness of Ti02 layer (cm)
xj1 = 50e-7;    %Thickness of Spiro-OMeTAD layer(cm)
Sn1 = 10000;       %Surface recombination velocity for electrons (cm/s)
Sp1 = 5.4;     %Surface recombination velocity for holes (cm/s)
Eg1 = 1.8;      %Band gap energy (eV)
Nc1 = 2.768e24;    %Conduction band carrier density for Si (cm-3)
Nv1 = 3.9194e24;   %Valence band carrier density for Si (cm-3)
T = 300;        %Temperature of solar cell (K)
H1 = W1+xj1+Hpr1;      %Total top cell thickness (cm)
lambda_Eg1 = h*c/(Eg1*q)*1e9;  %Wavelength w.r.t. Eg (nm)
```

```
%*****************************************************************
%Parameters of Bottom Material*************************************
Nd2 = 1e19;       %Donor density (cm-3)
Dp2 = 12.15;      %Hole diffusion coefficient in emitter (cm^{2}/s)
tp2 = 6.024e-9;      %Hole life time in emitter (s)
Lp2 = 2.7054e-4;   %Hole diffusion length in emitter (cm)
Na2 = 5e15;     %Acceptor density (cm-3)
Dn2 = 33.76;         %Electron diffusion coefficient in base (cm^{2}/s)
tn2 = 985.6e-6;  %Electron life time in base (s)
Ln2 = 1824e-4;      %Electron diffusion length in base (cm)
W2 = 280e-7;     %Depletion width (cm)
Hpr2 = 299.22e-4;       %Total cell thickness (cm)
xj2 = 500e-7;     %Junction depth of n+ region (cm)
Sn2 = 100;        %Surface recombination velocity for electrons (cm/s)
% For Back Surface Reflection region, Sn<100 cm/s according to
% SZE&NG, Physics of Semiconductor Devices, 3rd Edition, p.731
Sp2 = 1000;      %Surface recombination velocity for holes (cm/s)
Eg2 = 1.12;       %Band gap energy (eV)
Nc2 = 2.8e19;     %Conduction band carrier density for Si (cm-3)
Nv2 = 2.65e19;    %Valence band carrier density for Si (cm-3)
T = 300;         %Temperature of solar cell (K)
H2 = Hpr2+W2+xj2;    %Thickness of Silicon substrate (cm)
lambda_Eg2 = h*c/(Eg2*q)*1e9;  %Wavelength w.r.t. Eg (nm)
%*****************************************************************
V1 = linspace(0,2*Eg1,400);  %Voltage array for top cell
V2 = linspace(0,Eg2,400);  %Voltage array for bottom cell

%Load files containing material properties
%Excel files must contain a range of wavenlengths 300-1250nm in steps
of
%10nm
refFile = 'Reflectivity';  %File containing data for bare Silicon
refSheet = 'nank';
BSFile = 'BS_Reflectivity';  %File containing data for Black Silicon
BSSheet = 'Sheet1';
fluxFile = 'PhotonFlux';  %File containing data for Photon Flux
fluxSheet = 'Sheet1';
PerovFile = 'Perovskite';  %File containing data for Perovskite
PerovSheet = 'Sheet1';
SiNxFile = 'SiliconNitride';  %File containing data for Silicon Nitride
coating
SiNxSheet = 'SiNx_96nm';

choice = input('Enter "0" for series connection. Enter "1" for n-
terminal: ');
if choice==0
    disp('Series connection Tandem solar cell. ');
elseif choice==1
    disp('N-terminal Tandem solar cell. ');
else
    disp('Not a valid choice');
end

switch(choice)
    case 0
        %Change parameters of Top cell to match currents
```

```
        %Parameters of Top
Material************************************
        Nd1 = 3.17e20;      %Donor density (cm-3)
        Dp1 = .43056;     %Hole diffusion coefficient in emitter
(cm^{2}/s)
        tp1 = 16e-9;     %Hole life time in emitter (s)
        Lp1 = 830e-7;   %Hole diffusion length in emitter (cm)
        Na1 = 6.147e19;    %Acceptor density (cm-3)
        Dn1 = .42025;        %Electron diffusion coefficient in base
(cm^{2}/s)
        tn1 = 16e-9;  %Electron life time in base (s)
        Ln1 = 820e-7;     %Electron diffusion length in base (cm)
        W1 = 500e-7;    %Thickness of Perovskite layer (cm)
        Hpr1 = 200e-7;  %Thickness of TiO2 layer (cm)
        xj1 = 80e-7;    %Thickness of Spiro-OMeTAD layer(cm)
        Sn1 = 10000;       %Surface recombination velocity for
electrons (cm/s)
        % For Back Surface Field, Sn<100 cm/s according to
        % SZE&NG, Physics of Semiconductor Devices, 3rd Edition, p.731
        Sp1 = 5.4;     %Surface recombination velocity for holes (cm/s)
        Eg1 = 1.80;      %Band gap energy (eV)
        Nc1 = 2.768e24;    %Conduction band carrier density for Si (cm-
3)
        Nv1 = 3.9194e24;   %Valence band carrier density for Si (cm-3)
        T = 300;        %Temperature of solar cell (K)
        H1 = W1+xj1+Hpr1;      %Total top cell thickness (cm)
        lambda_Eg1 = h*c/(Eg1*q)*1e9;  %Wavelength w.r.t. Eg (nm)

%*****************************************************************
        x=input('Enter "0" for bare Silicon cell. Enter "1" for Black
Silicon cell. Enter "2" for Silicon Nitride coating: ');
        if(x==0)
            lambda = xlsread(refFile,refSheet,'A7:A102');  %Wavelength
300-1250nm
            n_Si = xlsread(refFile,refSheet,'D7:D102');  %Refractive
index of Silicon
            a_Si = xlsread(refFile,refSheet,'B7:B102');  %Absorption
coefficient of Silicon
            %Calculate reflectivity of bottom cell (silicon)
            R_Si = zeros(1,length(lambda));
            z = 1;
            while z<length(R_Si)
                R_Si(z) = ((n_Si(z)-n1)/(n_Si(z)+n1))^2;
                z = z+1;
            end
        end
        if(x==1)
            a_Si = xlsread(refFile,refSheet,'B7:B102');  %Absorption
coefficient of Silicon
            R_Si = xlsread(BSFile,BSSheet,'B5:B100');  %Reflectivity of
Black Silicon
            lambda = xlsread(refFile,refSheet,'A7:A102');  %Wavelength
300-1250nm
        end
        if(x==2)
           a_Si = xlsread(refFile,refSheet,'B7:B102');  %Absorption
coefficient of Silicon
```

```
            R_Si = xlsread(SiNxFile,SiNxSheet,'B6:B101');  %Reflectivity
of Silicon Nitride coating
            lambda = xlsread(refFile,refSheet,'A7:A102');  %Wavelength
300-1250nm
        end
        %Data from refractiveindex.info, Leguy et al. 2015
        n_perov = xlsread(PerovFile,PerovSheet,'J2:J97');  %Refractive
index of perovskite
        k_perov = xlsread(PerovFile,PerovSheet,'K2:K97');  %Extinction
coefficient of perovskite
        F = xlsread(fluxFile,fluxSheet,'B4:B99');  %Photon flux
(photons/s/m2/nm)
        %Calculate reflectivity of top cell (perovskite)
        R_perov = zeros(1,length(lambda));
        z = 1;
        while z<length(R_perov)
          R_perov(z) = ((n_perov(z)-n1)/(n_perov(z)+n1))^2;
          z = z+1;
        end

        %Calculate absorption of top cell (perovskite)
        a_perov = zeros(1,length(lambda));
        z = 1;
        while z<length(a_perov)
            a_perov(z) = 4*pi*k_perov(z)*1e7/lambda(z);
            z = z+1;
        end

        %Calculate photocurrent from emitter of top material
        Je1 = zeros(1,length(lambda));
        z = 1;
        while z<length(Je1)
            num_e1 = (Sn1*Ln1/Dn1+a_perov(z)*Ln1)-exp(-
a_perov(z)*xj1)*((Sn1*Ln1/Dn1)*cosh(xj1/Ln1)+sinh(xj1/Ln1));
            den_e1 = (Sn1*Ln1/Dn1)*sinh(xj1/Ln1)+cosh(xj1/Ln1);
            Je1(z) = (q*F(z)*(1-
R_perov(z))*a_perov(z)*Ln1)/(a_perov(z)^2*Ln1^2-1)*((num_e1/den_e1)-
(a_perov(z)*Ln1*exp(-a_perov(z)*xj1)));
            z = z+1;
        end
        %Calculate photocurrent from base of top material
        Jb1 = zeros(1,length(lambda));
        z = 1;
        while z<length(Jb1)
            num_b1 = (Sp1*Lp1/Dp1)*(cosh(Hpr1/Lp1)-exp(-
a_perov(z)*Hpr1))+sinh(Hpr1/Lp1)+a_perov(z)*Lp1*exp(-a_perov(z)*Hpr1);
            den_b1 = (Sp1*Lp1/Dp1)*sinh(Hpr1/Lp1)+cosh(Hpr1/Lp1);
            Jb1(z) = (q*F(z)*(1-
R_perov(z))*a_perov(z)*Lp1)/(a_perov(z)^2*Lp1^2-1)*exp(-
a_perov(z)*(xj1+W1))*(a_perov(z)*Lp1-(num_b1/den_b1));
            z = z+1;
        end
        %Calculate photocurrent from space charge region of top
material
        Jscr1 = zeros(1,length(lambda));
        z = 1;
        while z<length(Jscr1)
```

```
            Jscr1(z) = q*F(z)*(1-R_perov(z))*exp(-a_perov(z)*xj1)*(1-
exp(-a_perov(z)*W1));
            z = z+1;
        end
        %Calculate photocurrent from emitter of bottom material
        Je2 = zeros(1,length(lambda));
        z = 1;
        while z<length(Je2)
            num_e2 = (Sp2*Lp2/Dp2+a_Si(z)*Lp2)-exp(-
a_Si(z)*xj2)*((Sp2*Lp2/Dp2)*cosh(xj2/Lp2)+sinh(xj2/Lp2));
            den_e2 = (Sp2*Lp2/Dp2)*sinh(xj2/Lp2)+cosh(xj2/Lp2);
            Je2(z) = (q*F(z)*(1-R_Si(z))*a_Si(z)*Lp2)/(a_Si(z)^2*Lp2^2-
1)*((num_e2/den_e2)-(a_Si(z)*Lp2*exp(-a_Si(z)*xj2)));
            z = z+1;
        end
        %Calculate photocurrent from base of bottom material
        Jb2 = zeros(1,length(lambda));
        z = 1;
        while z<length(Jb2)
            num_b2 = (Sn2*Ln2/Dn2)*(cosh(Hpr2/Ln2)-exp(-
a_Si(z)*Hpr2))+sinh(Hpr2/Ln2)+a_Si(z)*Ln2*exp(-a_Si(z)*Hpr2);
            den_b2 = (Sn2*Ln2/Dn2)*sinh(Hpr2/Ln2)+cosh(Hpr2/Ln2);
            Jb2(z) = (q*F(z)*(1-R_Si(z))*a_Si(z)*Ln2)/(a_Si(z)^2*Ln2^2-
1)*exp(-a_Si(z)*(xj2+W2))*(a_Si(z)*Ln2-(num_b2/den_b2));
            z = z+1;
        end
        %Calculate photocurrent from space charge region of bottom
material
        Jscr2 = zeros(1,length(lambda));
        z = 1;
        while z<length(Jscr2)
            Jscr2(z) = q*F(z)*(1-R_Si(z))*exp(-a_Si(z)*xj2)*(1-exp(-
a_Si(z)*W2));
            z = z+1;
        end

        %Calculate internal quantum efficiency of top cell
        IQE1 = zeros(1,length(lambda));
        z = 1;
        while z<length(IQE1)
            IQE1(z) = (Je1(z)+Jb1(z)+Jscr1(z))/(q*F(z)*(1-R_perov(z)));
            z = z+1;
        end
        %Calculate internal quantum efficiency of bottom cell
        IQE2 = zeros(1,length(lambda));
        z = 1;
        while z<length(IQE2)
            %IQE2(z) = (Je2(z)+Jb2(z)+Jscr2(z))/(q*F(z)*(1-(R_Si(z)-
1+exp(-a_perov(z)*W1))));
            IQE2(z) = [(Je2(z)+Jb2(z)+Jscr2(z))*(exp(-
a_perov(z)*W1))]/(q*F(z)*(1-R_Si(z)));
            %dump(z) = exp(-a_perov(z)*W1)/(1-R_Si(z))
            z = z+1;
        end
        plot(lambda,100*IQE1,'m', 'Linewidth', 2); axis([280 1200 0
100]);
        hold on;
```

```
        plot(lambda,100*IQE2,'k', 'Linewidth', 2);
        title('Internal Quantum Efficiency vs. Wavelength');
        xlabel('Wavelength (nm)');
        ylabel('IQE(%)');
        hold on;
        plot(lambda, 100*R_Si, 'b', 'Linewidth', 2);
        hold on;
        plot(lambda, 100*R_perov, 'g', 'Linewidth', 2);
        hold on;
        plot(lambda,100*q*F,'y');
        legend('IQE Top Cell','IQE Bottom Cell', 'Si Reflectivity',
'Perovskite Reflectivity', 'Photon Flux');

        %Calculate external quantum efficiency of top cell
        EQE1 = zeros(1,length(lambda));
        z = 1;
        while z<length(EQE1)
            EQE1(z) = IQE1(z)*(1-R_perov(z));
            z = z+1;
        end
        %Calculate external quantum efficiency of bottom cell
        EQE2 = zeros(1,length(lambda));
        z = 1;
        while z<length(EQE2)
            EQE2(z) = IQE2(z)*(1-R_Si(z));
            EQEtemp(z) = EQE1(z)+EQE2(z);
            if(EQEtemp(z)>1)
                EQE2(z) = 1-EQE1(z);
            end
            z = z+1;
        end
        figure;
        plot(lambda,100*EQE1,'b', 'Linewidth', 2); axis([280 1200 0
1.5]);
        hold on;
        plot(lambda,100*EQE2,'k', 'Linewidth', 2);
        title('External Quantum Efficiency vs. Wavelength');
        xlabel('Wavelength (nm)');
        ylabel('EQE (%)');
        hold on;
        plot(lambda,q*F,'g');
        legend('EQE Top Cell','EQE Bottom Cell','Photon Flux');

        %Function inside photocurrent integral
        temp1 = zeros(1,length(lambda));
        z = 1;
        while z<length(temp1)
            temp1(z) = (1-R_perov(z))*F(z)*IQE1(z);
            z = z+1;
        end
        %Function inside photocurrent integral
        temp2 = zeros(1,length(lambda));
        z = 1;
        while z<length(temp2)
            temp2(z) = (1-R_Si(z))*F(z)*IQE2(z);
            z = z+1;
        end
```

```
        %Calculate photocurrent of top, bottom, and tandem cells
        bound1 = find(lambda<=lambda_Eg1,1,'last');
        Jph1 = q/10*trapz(lambda(1:bound1),temp1(1:bound1));  %Short
circuit current of top cell (mA/cm^{2})
        disp('Short circuit current of top cell (mA/cm^{2}): ');
disp(Jph1);
        bound2 = find(lambda<=lambda_Eg2,1,'last');
        Jph2 = Jph1;
        %Jph2 = q/10*trapz(lambda(1:bound2),temp2(1:bound2));  %Short
circuit current of bottom cell (mA/cm^{2})
        disp('Short circuit current of bottom cell (mA/cm^{2}): ');
disp(Jph2);
        Jph_total = Jph1+Jph2;  %Short circuit current of solar cell
(mA/cm^{2})
        disp('Total short circuit current (mA/cm^{2}): ');
disp(Jph_total);

        %Calculate dark current of top, bottom, and tandem cells
        Js1 =
1000*q*Nc1*Nv1*((sqrt(Dn1/tn1)/Na1)+(sqrt(Dp1/tp1)/Nd1))*exp((-
Eg1*q)/(k*T)); %Saturation current (mA/cm^{2})
        Jdark1 = Js1*(exp((q*V1)/(k*T))-1);  %Dark current of top cell
(mA/cm^{2})
        Js2 = Js1;
        %Js2 =
1000*q*Nc2*Nv2*((sqrt(Dn2/tn2)/Na2)+(sqrt(Dp2/tp2)/Nd2))*exp((-
Eg2*q)/(k*T)); %Saturation current (mA/cm^{2})
        Jdark2 = Js2*(exp((q*V2)/(k*T))-1);  %Dark current of bottom
cell (mA/cm^{2})
        Jdark_total = Jdark1+Jdark2;  %Total dark current of cell

        %Calculate open circuit voltage of top, bottom, and tandem
cells
        Voc1 = k*T/q*log(Jph1/Js1+1);  %Open circuit voltage of top
cell (V)
        Voc2 = k*T/q*log(Jph2/Js2+1);  %Open circuit voltage of bottom
cell (V)
        Voc_total = Voc1+Voc2;  %Total open circuit of cell
        disp('Open circuit voltage of top cell (V): '); disp(Voc1);
        disp('Open circuit voltage of bottom cell (V): '); disp(Voc2);
        disp('Total open circuit voltage (V): '); disp(Voc_total);

        J1 = Jph1-Js1*(exp((q*V1)/(k*T))-1); %Total current in top cell
(mA/cm^{2})
        J2 = Jph2-Js2*(exp((q*V2)/(k*T))-1); %Total current in bottom
cell (mA/cm^{2})
        J_total = J1+J2;  %Total solar cell current (mA/cm^{2})
        V_total = V1+V2;  %Total solar cell voltage (V)
        figure; plot(V1,J1,'b','Linewidth', 2); hold on;
plot(V2,J2,'g','Linewidth', 2); hold on; plot(V_total,J_total,'k',
'Linewidth', 2); axis([0 Voc_total+1 0 Jph_total+10]);
        title('Solar Cell Characteristic Curves');
        xlabel('Voltage (V)');
        ylabel('Current Density (mA/cm^{2})');

        P1 = V1.*J1;  %Power of top cell
        [PM1,loc1] = max(P1);
```

```
        P2 = V2.*J2;  %Power of bottom cell
        [PM2,loc2] = max(P2);
        P_total = V_total.*J_total;  %Power of tandem cell
        hold on;
        plot(V_total,P_total,'m', 'Linewidth', 2);
        [Pm,loc] = max(P_total);
        [row,col] = ind2sub(size(P_total),loc);
        Vm = V_total(col);  %Voltage at maximum power
        Jm = J_total(col);  %Current at maximum power
        hold on;
        plot(Vm,Jm,'om'); text(Vm,Jm,'  \leftarrow Maximum power
point', 'Linewidth', 2);
        legend('Top Cell','Bottom Cell','Tandem Cell','Power');
        disp('Maximum power (mW): '); disp(Pm);

        FF1 = 100*((q*Voc1/(k*T)-
log(q*Voc1/(k*T)+.72))/(q*Voc1/(k*T)+1));  %Fill factor of top cell
        FF2 = 100*((q*Voc2/(k*T)-
log(q*Voc2/(k*T)+.72))/(q*Voc2/(k*T)+1));  %Fill factor of bottom cell
        FF_total = 100*((q*Voc_total/(k*T)-
log(q*Voc_total/(k*T)+.72))/(q*Voc_total/(k*T)+1));  %Fill factor of
tandem cell
        disp('Fill factor of top cell (%): '); disp(FF1);
        disp('Fill factor of bottom cell (%): '); disp(FF2);
        disp('Fill factor of tandem cell (%): '); disp(FF_total);

        eff1 = 100*PM1/100.4;  %Efficiency of top cell
        eff2 = 100*PM2/100.4;  %Efficiency of bottom cell
        eff_total =
(100/100.4)*((FF1/100*Voc1*Jph1)+(FF2/100*Voc2*Jph2));  %Efficiency of
tandem cell (%)
        disp('Efficiency of top cell (%): '); disp(eff1);
        disp('Efficiency of bottom cell (%): '); disp(eff2);
        disp('Efficiency of tandem cell (%): '); disp(eff_total);

    case 1
        x=input('Enter "0" for Silicon cell. Enter "1" for Black
Silicon cell. Enter "2" for Silicon Nitride coating: ');
        if(x==0)
            lambda = xlsread(refFile,refSheet,'A7:A102');  %Wavelength
300-1250nm
            n_Si = xlsread(refFile,refSheet,'D7:D102');  %Refractive
index of Silicon
            a_Si = xlsread(refFile,refSheet,'B7:B102');  %Absorption
coefficient of Silicon
            %Calculate reflectivity of bottom cell (silicon)
            R_Si = zeros(1,length(lambda));
            z = 1;
            while z<length(R_Si)
                R_Si(z) = ((n_Si(z)-n1)/(n_Si(z)+n1))^2;
                z = z+1;
            end
        end
        if(x==1)
            a_Si = xlsread(refFile,refSheet,'B7:B102');  %Absorption
coefficient of Silicon
```

```
            R_Si = xlsread(BSFile,BSSheet,'B5:B100');  %Reflectivity of
Black Silicon
            lambda = xlsread(refFile,refSheet,'A7:A102');  %Wavelength
300-1250nm
        end
        if(x==2)
           a_Si = xlsread(refFile,refSheet,'B7:B102');  %Absorption
coefficient of Silicon
            R_Si = xlsread(SiNxFile,SiNxSheet,'B6:B101');  %Reflectivity
of Silicon Nitride coating
            lambda = xlsread(refFile,refSheet,'A7:A102');  %Wavelength
300-1250nm
        end
        %Data from refractiveindex.info, Leguy et al. 2015
        n_perov = xlsread(PerovFile,PerovSheet,'J2:J97');  %Refractive
index of perovskite
        k_perov = xlsread(PerovFile,PerovSheet,'K2:K97');  %Extinction
coefficient of perovskite
        F = xlsread(fluxFile,fluxSheet,'B4:B99');  %Photon flux
(photons/s/m2/nm)
        %Calculate reflectivity of top cell (perovskite)
        R_perov = zeros(1,length(lambda));
        z = 1;
        while z<length(R_perov)
          R_perov(z) = ((n_perov(z)-n1)/(n_perov(z)+n1))^2;
          z = z+1;
        end

        %Calculate absorption of top cell (perovskite)
        a_perov = zeros(1,length(lambda));
        z = 1;
        while z<length(a_perov)
            a_perov(z) = 4*pi*k_perov(z)*1e7/lambda(z);
            z = z+1;
        end
        %Calculate photocurrent from emitter of top material
        Je1 = zeros(1,length(lambda));
        z = 1;
        while z<length(Je1)
            num_e1 = (Sn1*Ln1/Dn1+a_perov(z)*Ln1)-exp(-
a_perov(z)*xj1)*((Sn1*Ln1/Dn1)*cosh(xj1/Ln1)+sinh(xj1/Ln1));
            den_e1 = (Sn1*Ln1/Dn1)*sinh(xj1/Ln1)+cosh(xj1/Ln1);
            Je1(z) = (q*F(z)*(1-
R_perov(z))*a_perov(z)*Ln1)/(a_perov(z)^2*Ln1^2-1)*((num_e1/den_e1)-
(a_perov(z)*Ln1*exp(-a_perov(z)*xj1)));
            z = z+1;
        end
        %Calculate photocurrent from base of top material
        Jb1 = zeros(1,length(lambda));
        z = 1;
        while z<length(Jb1)
            num_b1 = (Sp1*Lp1/Dp1)*(cosh(Hpr1/Lp1)-exp(-
a_perov(z)*Hpr1))+sinh(Hpr1/Lp1)+a_perov(z)*Lp1*exp(-a_perov(z)*Hpr1);
            den_b1 = (Sp1*Lp1/Dp1)*sinh(Hpr1/Lp1)+cosh(Hpr1/Lp1);
            Jb1(z) = (q*F(z)*(1-
R_perov(z))*a_perov(z)*Lp1)/(a_perov(z)^2*Lp1^2-1)*exp(-
a_perov(z)*(xj1+W1))*(a_perov(z)*Lp1-(num_b1/den_b1));
```

```
            z = z+1;
        end
        %Calculate photocurrent from space charge region of top
material
        Jscr1 = zeros(1,length(lambda));
        z = 1;
        while z<length(Jscr1)
            Jscr1(z) = q*F(z)*(1-R_perov(z))*exp(-a_perov(z)*xj1)*(1-
exp(-a_perov(z)*W1));
            z = z+1;
        end
        %Calculate photocurrent from emitter of bottom material
        Je2 = zeros(1,length(lambda));
        z = 1;
        while z<length(Je2)
            num_e2 = (Sp2*Lp2/Dp2+a_Si(z)*Lp2)-exp(-
a_Si(z)*xj2)*((Sp2*Lp2/Dp2)*cosh(xj2/Lp2)+sinh(xj2/Lp2));
            den_e2 = (Sp2*Lp2/Dp2)*sinh(xj2/Lp2)+cosh(xj2/Lp2);
            Je2(z) = (q*F(z)*(1-R_Si(z))*a_Si(z)*Lp2)/(a_Si(z)^2*Lp2^2-
1)*((num_e2/den_e2)-(a_Si(z)*Lp2*exp(-a_Si(z)*xj2)));
            z = z+1;
        end
        %Calculate photocurrent from base of bottom material
        Jb2 = zeros(1,length(lambda));
        z = 1;
        while z<length(Jb2)
            num_b2 = (Sn2*Ln2/Dn2)*(cosh(Hpr2/Ln2)-exp(-
a_Si(z)*Hpr2))+sinh(Hpr2/Ln2)+a_Si(z)*Ln2*exp(-a_Si(z)*Hpr2);
            den_b2 = (Sn2*Ln2/Dn2)*sinh(Hpr2/Ln2)+cosh(Hpr2/Ln2);
            Jb2(z) = (q*F(z)*(1-R_Si(z))*a_Si(z)*Ln2)/(a_Si(z)^2*Ln2^2-
1)*exp(-a_Si(z)*(xj2+W2))*(a_Si(z)*Ln2-(num_b2/den_b2));
            z = z+1;
        end
        %Calculate photocurrent from space charge region of bottom
material
        Jscr2 = zeros(1,length(lambda));
        z = 1;
        while z<length(Jscr2)
            Jscr2(z) = q*F(z)*(1-R_Si(z))*exp(-a_Si(z)*xj2)*(1-exp(-
a_Si(z)*W2));
            z = z+1;
        end

        %Calculate internal quantum efficiency of top cell
        IQE1 = zeros(1,length(lambda));
        z = 1;
        while z<length(IQE1)
            IQE1(z) = (Je1(z)+Jb1(z)+Jscr1(z))/(q*F(z)*(1-R_perov(z)));
            z = z+1;
        end
        %Calculate internal quantum efficiency of bottom cell
        IQE2 = zeros(1,length(lambda));
        z = 1;
        while z<length(IQE2)
            IQE2(z) = [(Je2(z)+Jb2(z)+Jscr2(z))*exp(-
a_perov(z)*W1)]/(q*F(z)*(1-(R_Si(z))));
            z = z+1;
```

```
        end
        plot(lambda,100*IQE1,'m', 'Linewidth', 2); axis([280 1200 0
100]);
        hold on;
        plot(lambda,100*IQE2,'k', 'Linewidth',2);
        title('Internal Quantum Efficiency vs. Wavelength');
        xlabel('Wavelength (nm)');
        ylabel('IQE(%)');
        hold on;
        plot(lambda, 100*R_Si, 'b', 'Linewidth', 2);
        hold on;
        plot(lambda, 100*R_perov, 'g', 'Linewidth', 2);
        hold on;
        plot(lambda,100*q*F,'c');
        legend('IQE Top Cell','IQE Bottom Cell', 'Si Reflectivity',
'Perovskite Reflectivity', 'Photon Flux');

        %Calculate external quantum efficiency of top cell
        EQE1 = zeros(1,length(lambda));
        z = 1;
        while z<length(EQE1)
            EQE1(z) = IQE1(z)*(1-R_perov(z));
            z = z+1;
        end
        %Calculate external quantum efficiency of bottom cell
        EQE2 = zeros(1,length(lambda));
        z = 1;
        while z<length(EQE2)
            EQE2(z) = IQE2(z)*(1-R_Si(z));
            EQEtemp(z) = EQE1(z)+EQE2(z);
            if(EQEtemp(z)>1)
                EQE2(z) = 1-EQE1(z);
            end
            z = z+1;
        end
        figure;
        plot(lambda,EQE1,'b', 'Linewidth', 2); axis([280 1200 0 1]);
        hold on;
        plot(lambda,EQE2,'k', 'Linewidth', 2);
        title('External Quantum Efficiency vs. Wavelength');
        xlabel('Wavelength (nm)');
        ylabel('EQE');
        hold on;
        plot(lambda,q*F,'g');
        legend('EQE Top Cell','EQE Bottom Cell','Photon Flux');

        %Function inside photocurrent integral
        temp1 = zeros(1,length(lambda));
        z = 1;
        while z<length(temp1)
            temp1(z) = (1-R_perov(z))*F(z)*IQE1(z);
            z = z+1;
        end
        %Function inside photocurrent integral
        temp2 = zeros(1,length(lambda));
        z = 1;
        while z<length(temp2)
```

```
            temp2(z) = (1-R_Si(z))*F(z)*IQE2(z);
            z = z+1;
        end
        %Calculate photocurrent of top, bottom, and tandem cells
        bound1 = find(lambda<=lambda_Eg1,1,'last');
        Jph1 = q/10*trapz(lambda(1:bound1),temp1(1:bound1));  %Short
circuit current of top cell (mA/cm^{2})
        disp('Short circuit current of top cell (mA/cm^{2}): ');
disp(Jph1);
        bound2 = find(lambda<=lambda_Eg2,1,'last');
        Jph2 = q/10*trapz(lambda(1:bound2),temp2(1:bound2));  %Short
circuit current of bottom cell (mA/cm^{2})
        disp('Short circuit current of bottom cell (mA/cm^{2}): ');
disp(Jph2);
        Jph_total = Jph1+Jph2;  %Short circuit current of solar cell
(mA/cm^{2})
        disp('Total short circuit current (mA/cm^{2}): ');
disp(Jph_total);

        %Calculate dark current of top, bottom, and tandem cells
        Js1 =
1000*q*Nc1*Nv1*((sqrt(Dn1/tn1)/Na1)+(sqrt(Dp1/tp1)/Nd1))*exp((-
Eg1*q)/(k*T)); %Saturation current (mA/cm^{2})
        Jdark1 = Js1*(exp((q*V1)/(k*T))-1);  %Dark current of top cell
(mA/cm^{2})
        Js2 =
1000*q*Nc2*Nv2*((sqrt(Dn2/tn2)/Na2)+(sqrt(Dp2/tp2)/Nd2))*exp((-
Eg2*q)/(k*T)); %Saturation current (mA/cm^{2})
        Jdark2 = Js2*(exp((q*V2)/(k*T))-1);  %Dark current of bottom
cell (mA/cm^{2})
        Jdark_total = Jdark1+Jdark2;  %Total dark current of cell

        %Calculate open circuit voltage of top, bottom, and tandem
cells
        Voc1 = k*T/q*log(Jph1/Js1+1);  %Open circuit voltage of top
cell (V)
        Voc2 = k*T/q*log(Jph2/Js2+1);  %Open circuit voltage of bottom
cell (V)
        Voc_total = Voc1+Voc2;  %Total open circuit of cell
        disp('Open circuit voltage of top cell (V): '); disp(Voc1);
        disp('Open circuit voltage of bottom cell (V): '); disp(Voc2);
        disp('Total open circuit voltage (V): '); disp(Voc_total);

        J1 = Jph1-Js1*(exp((q*V1)/(k*T))-1); %Total current in top cell
(mA/cm^{2})
        J2 = Jph2-Js2*(exp((q*V2)/(k*T))-1); %Total current in bottom
cell (mA/cm^{2})
        J_total = J1+J2;  %Total solar cell current (mA/cm^{2})
        V_total = V1+V2;  %Total solar cell voltage (V)
        figure; plot(V1,J1,'b','Linewidth', 2); hold on;
plot(V2,J2,'g','Linewidth', 2); hold on; plot(V_total,J_total,'k',
'Linewidth', 2); axis([0 Voc_total+1 0 Jph_total+10]);
        title('Solar Cell Characteristic Curves');
        xlabel('Voltage (V)');
        ylabel('Current Density (mA/cm^{2})');

        P1 = V1.*J1;  %Power of top cell
```

```
        [PM1,loc1] = max(P1);
        P2 = V2.*J2;  %Power of bottom cell
        [PM2,loc2] = max(P2);
        P_total = V_total.*J_total;  %Power of tandem cell
        hold on;
        plot(V_total,P_total,'m', 'Linewidth', 2);
        [Pm,loc] = max(P_total);
        [row,col] = ind2sub(size(P_total),loc);
        Vm = V_total(col);  %Voltage at maximum power
        Jm = J_total(col);  %Current at maximum power
        hold on;
        plot(Vm,Jm,'om', 'Linewidth', 2); text(Vm,Jm,'  \leftarrow
Maximum power point');
        legend('Top Cell','Bottom Cell','Tandem Cell','Power');
        disp('Maximum power (mW): '); disp(Pm);

        FF1 = 100*((q*Voc1/(k*T)-
log(q*Voc1/(k*T)+.72))/(q*Voc1/(k*T)+1));  %Fill factor of top cell
        FF2 = 100*((q*Voc2/(k*T)-
log(q*Voc2/(k*T)+.72))/(q*Voc2/(k*T)+1));  %Fill factor of bottom cell
        FF_total = 100*((q*Voc_total/(k*T)-
log(q*Voc_total/(k*T)+.72))/(q*Voc_total/(k*T)+1));  %Fill factor of
tandem cell
        disp('Fill factor of top cell (%): '); disp(FF1);
        disp('Fill factor of bottom cell (%): '); disp(FF2);
        disp('Fill factor of tandem cell (%): '); disp(FF_total);

        eff1 = 100*PM1/100.4;  %Efficiency of top cell
        eff2 = 100*PM2/100.4;  %Efficiency of bottom cell
        eff_total =
(100/100.4)*((FF1/100*Voc1*Jph1)+(FF2/100*Voc2*Jph2));  %Efficiency of
tandem cell (%)
        disp('Efficiency of top cell (%): '); disp(eff1);
        disp('Efficiency of bottom cell (%): '); disp(eff2);
        disp('Efficiency of tandem cell (%): '); disp(eff_total);
end
```

Matlab Code for DAR SiN_x Reflection Model

```
%Author: Lauren Davidson
%Date: 02-06-2017
%Description: This program models a Si cell with a double anti-
reflective
%(DAR) coating. It figures out the reflectivity based on the refractive
%index and thickness of each layer.

clear all;
close all;

%Load Excel file with reflectivity data of bare Si
refFile = 'Reflectivity';
refSheet = 'nank';
%Load Excel file with photon flux data
fluxFile = 'PhotonFlux';
fluxSheet = 'Sheet1';
```

```
%Photon flux from wavelengths of 300-1200nm in increments of 10nm
F = xlsread(fluxFile,fluxSheet,'B4:B94');
%Refractive index of bare Silicon from wavelengths 0f 300-1200nm in
%increments of 10nm
n_Si = xlsread(refFile,refSheet,'D7:D97');
%Wavelengths 300-1200nm in 10nm increments
lambda = xlsread(refFile,refSheet,'A7:A97');
lambda = lambda'*1e-9;
%Refractive index of air
n0 = 1;
%Reflectivity of bare Si cell
R_Si = zeros(1,length(n_Si));
%Charge of electron
q = 1.602e-19;

for i = 1:length(R_Si)
    R_Si(i) = ((n_Si(i)-n0)/(n_Si(i)+n0))^2;
end

%Set material parameters
%-----------------------
%Refractive index of top layer
n1 = 1.75;
%Refractive index of middle layer
n2 = 2.0;
%Refractive index of Si substrate
n3 = 3.42;

%Optimizing depths of AR coatings for specific wavelength in nm
lambda1 =600;
lambda1 = lambda1*1e-9;
lambda2 = 600;
lambda2 = lambda2*1e-9;

%Bound limits for surface
bound1 = (lambda<700*1e-9);
bound2 = (lambda>500*1e-9);
bound = bound1.*bound2;

%Number of iterations
num = length(lambda);

%Starting layer thicknesses
t1_start = 35*1e-9;
t2_start = 20*1e-9;

for j=1:num
%Thickness of middle layer
t2(j) = t2_start + (j-1)*1e-9;
for i=1:num
%Thickness of top layer in nm
t1(i) = t1_start + (i-1)*1e-9;

r1 = (n0-n1)/(n0+n1);
r2 = (n1-n2)/(n1+n2);
r3 = (n2-n3)/(n2+n3);
theta1 = 2*pi*n1*t1(i)./lambda;
```

```
theta2 = 2*pi*n2*t2(j)./lambda;

%Reflectance numerator
num =
r1^2+r2^2+r3^2+r1^2*r2^2*r3^2+2*r1*r2*(1+r3^2)*cos(2.*theta1)+2*r2*r3*(
1+r1^2)*cos(2.*theta2)+2*r1*r3*cos(2.*(theta1+theta2))+2*r1*r2^2*r3*cos
(2.*(theta1-theta2));
%Reflectance denominator
den =
1+r1^2*r2^2+r1^2*r3^2+r2^2*r3^2+2*r1*r2*(1+r3^2)*cos(2.*theta1)+2*r2*r3
*(1+r1^2)*cos(2.*theta2)+2*r1*r3*cos(2.*(theta1+theta2))+2*r1*r2^2*r3*c
os(2.*(theta1-theta2));

%Bounded Reflectance Mesh
% R(i,:) = bound.*(num./den);

%Unbounded Reflectance Mesh
R(i,:) = num./den;
i = i+1;
end
T(j,:) = lambda*1e9;
j = j+1;
end

figure; mesh(t1*1e9,t2*1e9,R*100,T);
title('Optimized DAR SiNx Layer Thicknesses');
xlabel('Top Layer Thickness (nm)');
ylabel('Bottom Layer Thickness (nm)');
zlabel('Reflectivity (%)');
c = colorbar;
c.Label.String = 'Wavelength (nm)';
colormap jet;

%Average reflectivity
Ravg_Si = mean(R_Si);
Ravg_DAR = mean(R);
T = ['Average reflectivity of Si: Ravg = ',num2str(Ravg_Si*100),' %'];
disp(T);
S = ['Average reflectivity DAR coatings: Ravg =
',num2str(Ravg_DAR*100),' %'];
disp(S);
```

REFERENCES

1. Green, M.A., et al., *Solar cell efficiency tables (version 48).* Progress in Photovoltaics: Research and Applications, 2016. **24**(7): p. 905-913.

2. Kayes, B.M., et al., *27.6% Conversion efficiency, a new record for single-junction solar cells under 1 sun illumination*, in *2011 37th IEEE Photovoltaic Specialists Conference*. 2011.

3. *PV Spot Price*. 2015, EnergyTrend, a Business Division of TrendForce Corp.

4. Toor, F., et al., *Multi-scale surface texture to improve blue response of nanoporous black silicon solar cells.* Applied Physics Letters, 2011. **99**(10): p. 3.

5. Toor, F., et al., *Metal assisted catalyzed etched (MACE) black Si: optics and device physics.* Nanoscale, 2016. **8**(34): p. 15448-15466.

6. Toor, F., et al., *Nanostructured silicon via metal assisted catalyzed etch (MACE): chemistry fundamentals and pattern engineering.* Nanotechnology, 2016. **27**(41).

7. Toor, F., J. Oh, and H.M. Branz, *Efficient nanostructured 'black' silicon solar cell by copper-catalyzed metal-assisted etching.* Progress in Photovoltaics: Research and Applications, 2014: p. n/a-n/a.

8. Tang, Y., et al., *N+ emitters realized using Ammonium Dihydrogen Phosphate for silicon solar cells.* Solar Energy, 2013. **95**: p. 265-270.

9. Sze, S.M. and K.K. NG, *Physics of Semiconductor Devices*. 3rd ed. 2007, Hoboken, New Jersey: John Wiley & Sons, Inc.

10. Parikh, V.Y. and T.U.o. Toledo, *Studies of Two-terminal and Four-terminal Polycrystalline Thin Film Tandem Solar Cells Based on II-VI Materials*. 2007, The University of Toledo.

11. Kojima, A., et al., *Organometal Halide Perovskites as Visible-Light Sensitizers for Photovoltaic Cells.* Journal of the American Chemical Society, 2009. **131**(17): p. 6050-+.

12. Green, M.A., A. Ho-Baillie, and H.J. Snaith, *The emergence of perovskite solar cells.* Nature Photonics, 2014. **8**(7): p. 506-514.

13. Chilvery, A.K., et al., *Perovskites: transforming photovoltaics, a mini-review.* Journal of Photonics for Energy, 2015. **5**.

14. Duerinckx, F. and J. Szlufcik, *Defect passivation of industrial multicrystalline solar cells based on PECVD silicon nitride.* Solar Energy Materials and Solar Cells, 2002. **72**(1-4): p. 231-246.

15. Han, S.S., et al., *Preparation of a-SiNx thin film with low hydrogen content by inductively coupled plasma enhanced chemical vapor deposition.* Journal of the Electrochemical Society, 1998. **145**(2): p. 652-658.

16. Yoo, J., et al., *Study on hydrogenated silicon nitride for application of high efficiency crystalline silicon solar cells.* Solar Energy Materials and Solar Cells, 2011. **95**(1): p. 7-10.

17. Vetter, M., *Surface passivation of silicon by rf magnetron-sputtered silicon nitride films.* Thin Solid Films, 1999. **337**(1-2): p. 118-122.

18. Honsberg, C. and S. Bowden. *Anti-Reflection Coatings*. Design of Silicon Cells 2013; Available from: http://pveducation.org/pvcdrom/anti-reflection-coatings.

19. Sahouane, N. and A. Zerga, *Optimization of Antireflection Multilayer for Industrial Crystalline Silicon Solar Cells.* Energy Procedia, 2014. **44**: p. 118-125.

20. Du, G.P., et al., *Performance enhancement of multicrystalline silicon solar cells and modules using double-layered SiNx: H antireflection coatings.* Progress in Photovoltaics, 2015. **23**(12): p. 1806-1814.

21. Honsberg, C. and S. Bowden. *Silicon Solar Cell Parameters*. Solar Cell Structure 2013; Available from: http://pveducation.org/pvcdrom/design/solar-cell-parameters.